FERMI AND NON–FERMI LIQUID BEHAVIOR IN QUANTUM IMPURITY SYSTEMS: CONSERVING SLAVE BOSON THEORY*

Johann Kroha and Peter Wölfle

Institut für Theorie der Kondensierten Materie, Universität Karlsruhe, Postfach 6980, 76128 Karlsruhe, Germany

(Received February 1, 2008)

The question of Fermi liquid vs. non–Fermi liquid behavior induced by strong correlations is one of the prominent problems in metallic local moment systems. As standard models for such systems, the SU(N)×SU(M) Anderson impurity models exhibit both Fermi liquid and non–Fermi liquid behavior, depending on their symmetry. Taking the Anderson model as an example, these lectures first give an introduction to the auxiliary boson method to describe correlated systems governed by a strong, short–range electronic repulsion. It is then shown how to include the relevant low–lying excitations (coherent spin flip and charge fluctuation processes), while preserving the local gauge symmetry of the model. This amounts to a conserving T–matrix approximation (CTMA). We prove a cancellation theorem showing that the CTMA incorporates all leading and subleading infrared singularities at *any* given order in a self–consistent loop expansion of the free energy. As a result, the CTMA recovers the correct infrared behavior of the auxiliary particle propagators, indicating that it correctly describes both the Fermi and the non–Fermi regimes of the Anderson model.

PACS numbers: 71.27.+a, 71.10.Fd, 71.28.+d, 75.20.Hr

1. Introduction

It is a remarkable feature of interacting, itinerant fermion systems that at low temperatures T they behave in general in much the same way as a noninteracting Fermi gas, even though the interaction may be strong. An extremely successful description of this phenomenon, known as Fermi liquid (FL) behavior, is provided by the notion of quasiparticles, which was established by Landau's phenomenological Fermi liquid theory [1]. The

* Lectures presented at the XXXVIII Cracow School of Theoretical Physics, June 1–10, 1998, Zakopane, Poland.

key assumption is that, as the interaction is continuously turned on, there exists a 1:1 correspondence between the low energy eigenstates of the interacting system and the single–particle states of the free Fermi gas. Therefore, the low–lying interacting states may be described approximately as single–particle states or quasiparticles, whose decay rate $1/\tau$ is small compared to their excitation energy ω, $1/\tau \ll \omega$, and which are characterized by the same quantum numbers as the noninteracting states. As a consequence, Fermi liquids exhibit the same low–T thermodynamics as a noninteracting Fermi system, e.g. a linear in T specific heat $c = \gamma T$ and a constant Pauli paramagnetic susceptibility χ_o. However, the effective mass and other parameters may be renormalized by the interaction, resulting in an enhancement of the specific heat coefficient γ and the susceptibility χ_o. It is at the heart of the quasiparticle picture that at low T the Pauli exclusion principle substantially reduces the phase space available to quasiparticle scattering. This blocking mechanism is effective as long as the quasiparticle interaction is *shortranged in space and time*, which is usually the case in three dimensions because of screening. It also implies that the quasiparticle scattering rate vanishes as $1/\tau \propto (\omega^2 + T^2)$ in the limit $\omega,\ T \to 0$, thus providing a microscopic justification for the basic assumption of FL theory and leading to an interaction contribution to the electrical resistivity which behaves as $\Delta\rho \propto T^2$. Obviously, the Pauli principle as the origin of FL behavior is very robust, which explains the almost ubiquitous presence of a FL ground state in interacting Fermi systems and the broad success of Fermi liquid theory.

In this light it is all the more exciting that in recent years a number of new alloys have been discovered which exhibit striking deviations from this usual behavior. These systems have in common that a localized, degenerate degree of freedom, the magnetic moment of a magnetic ion, is dynamically coupled to a continuum of conduction electron states. In general, such a coupling generates the Kondo effect, characterized by resonant spin flip scattering of electrons at the Fermi surface off the local moment. Concomitantly, the conduction electron spin flip rate initially increases logarithmically as the temperature is lowered, passes through a maximum at a characteristic scale, the Kondo temperature T_K, and approaches zero as $T \to 0$, because the effective local moment becomes screened by the conduction electron spins. Thus, even for many strongly correlated systems of this type a Fermi liquid description applies below T_K, with usually a strongly enhanced quasiparticle effective mass, lending the term "heavy fermion systems" to these materials.

Completely new physics may arise, however, if the quenching of the local moments is inhibited. Two different mechanisms for the appearance of a non–Fermi liquid ground state have been put forward:

(1) Proximity of a quantum phase transition (QPT) to an antiferromag-

netically ordered state [2]–[5] as a function of a dopant concentration x or of pressure. Near the QPT the quantum critical fluctuations become longranged in space and time and can, thus, mediate a longrange quasiparticle interaction, leading to a breakdown of FL theory. There are indications for this spatially extended mechanism to be realized near the QPT of certain Ce based compounds like $CeCu_{6-x}Au_x$ [6, 7], $CeCu_2Si_2$ [8], and $CePd_2Si_2$ [9, 10].

(2) Two–channel Kondo effect (2CK) [11, 12]. The local magnetic moment is coupled to two exactly degenerate conduction electron channels. Because of a frustration effect between the screening of the local moment by the different conduction channels the moment quenching cannot be complete, leading to a nonvanishing conduction electron spin scattering rate even at the lowest temperatures and subsequently to a breakdown of FL behavior. It has been suggested [13] that this mechanism, based on single–ion dynamics rather than longrange fluctuations, may be realized predominantly in U based materials with cubic symmetry about the magnetic ion, such as $Y_{1-x}U_xPd_3$ [14] or $UCu_{5-x}Pt_x$ [15], which do not exhibit a QPT.

In both scenarios the wealth of experimental data showing non–FL behavior at low temperatures is not consistently explained by the present theories. Open questions within the QPT picture include, e.g., whether the local impurity dynamics competing with the magnetic ordering can play a role, and how the transition from the spin screened heavy FL phase to the magnetically ordered phase occurs alltogether. In the 2CK mechanism, on the other hand, inter–impurity interactions could modify the single ion behavior. Exact solution methods as well as numerical simulations have provided important progress in our understanding of strongly correlated quantum impurity systems. However, their applicability is essentially restricted to problems involving only a single impurity, owing to integrability conditions or limitations in the numerical effort, respectively. Therefore, more generally applicable theoretical techniques are called for.

In the present work we focus on the single–ion dynamics. We develop a standard field theoretical method, based on an auxiliary particle or slave boson representation, which describes the quantum impurity dynamics in a controlled way and at the same time has the potential of being extended to problems of many impurities on a lattice. As a standard model of strongly correlated electrons which, depending on its symmetry, exhibits both FL and non–FL behavior, we consider the SU(N)×SU(M) Anderson impurity model of a local, N–fold degenerate degree of freedom, coupled to M identical conduction bands.

In order to set the stage for the more formal development of the theory, in the following section we will briefly review the striking differences in the phenomenology of the single–channel and the multi–channel Kondo effects. In section 3 the slave boson representation is introduced, which provides a particularly compact formulation of the SU(N)×SU(M) Anderson model. We also discuss why the presence of FL or non–FL behavior in a given quantum impurity system can already be seen from the singular infrared dynamics of the auxiliary particles. Section 4 contains a critical assessment of earlier approximate slave boson treatments. This will motivate our conserving slave boson approach (conserving T–matrix approximation, CTMA), which is developed in section 5. As will be seen, the results produced from this theory are in very good agreement with known exact properties of the model. Conclusions are drawn in section 6. In the appendices we prove a cancellation theorem for non–CTMA diagrams, which justifies the CTMA on formal grounds, and derive in detail the self–consistent CTMA equations.

2. Single– and multi–channel Kondo effect and possible physical realizations

In this section we briefly discuss how the single–channel and the two–channel Kondo effects may arise in magnetic metals, if the interaction between the local moments can be neglected. We first discuss the usual magnetic, single–channel Kondo effect. A local moment is generated by an atomic f or d level whose energy E_d lies far below the Fermi energy $\varepsilon_F \equiv 0$ and whose electron occupation number is effectively restricted to $n_d \leq 1$ by a strong Coulomb repulsion U between two electrons in the same orbital. While the angular momentum degeneracy of the level is usually lifted by crystal field splitting, in the absence of a magnetic field a twofold degeneracy of a level occupied by one electron is guaranteed by time reversal symmetry (Kramers doublet), corresponding to the spin quantum numbers $m = \pm 1/2$ of the electron. In addition, there is a hybridization matrix element V between the atomic orbital and the conduction electron states. Such a system is described by the single impurity Anderson Hamiltonian

$$H = \sum_{\vec{k},\sigma} \varepsilon_{\vec{k}} c^\dagger_{\vec{k}\sigma} c_{\vec{k}\sigma} + E_d \sum_\sigma d^\dagger_\sigma d_\sigma + V \sum_{\vec{k},\sigma} (c^\dagger_{\vec{k}\sigma} d_\sigma + h.c.) + U d^\dagger_\uparrow d_\uparrow d^\dagger_\downarrow d_\downarrow, \quad (2.1)$$

where $c^\dagger_{\vec{k}\sigma}$ and $d^\dagger_\sigma$ are the creation operators of a conduction electron with dispersion $\varepsilon_{\vec{k}}$ and of an electron in the local orbital with spin σ, respectively. The low energy physics of this system is dominated by processes of second order in V, by which an electron hybridizes with the conduction band and the

impurity level is subsequently filled by another electron, thereby effectively flipping the impurity spin. Thus, in the region of low excitation energies, the Anderson Hamiltonian (2.1) may be mapped onto the s–d exchange (or Kondo) model [16], the effective coupling between the impurity spin and the conduction electron spin always being antiferromagnetic: $J = |V|^2/|E_d| > 0$ ($U \gg |E_d|$). These models have been studied extensively by means of Wilson's renormalization group [17], by the Bethe ansatz method [18, 19] and by means of a phenomenological Fermi liquid theory [20]. In this way the following physical picture has emerged: The model contains a dynamically generated low temperature scale, the Kondo temperature, which is expressed in terms of the parameters of the Anderson Hamiltonian (2.1) as $T_K = D(N\Gamma/D)^{(M/N)}\exp\{-\pi E_d/(N\Gamma)\}$, with $\mathcal{N}(0)$ and $D = 1/\mathcal{N}(0)$ the density of states at the Fermi energy and the high energy band cutoff, respectively. $\Gamma = \pi V^2\mathcal{N}(0)$ denotes the effective hybridization or d–level broadening and N, M are the degeneracy of the local level and the number of conduction electron channels (see below). In the intermediate temperature regime, $T \gtrsim T_K$, resonant spin flip scattering of electrons at the Fermi surface off the local degenerate level leads to logarithmic contributions to the magnetic susceptibility, the linear specific heat coefficient and the resistivity ($\rho(T) = \rho(0) + \Delta\rho(T)$), $\chi(T)$, $\gamma(T)$, $\Delta\rho(T) \propto -\ln(T/T_K)$, and to a breakdown of perturbation theory at $T \simeq T_K$. Below T_K a collective many–body spin singlet state develops in which the impurity spin is screened by the conduction electron spins as lower and lower energy scales are successively approached, leaving the system with a pure potential scattering center. The spin singlet formation is sketched in Fig. 1 a) and corresponds to a vanishing entropy at $T = 0$, $S(0) = 0$. It also leads to saturated behavior of physical quantities below T_K, like $\chi(T) = const.$, $c(T)/T = const.$ and $\Delta\rho(T) \propto T^2$, i.e. to Fermi liquid behavior.

As an example of possible two–channel Kondo systems we discuss the uranium based compounds mentioned in the introduction. The U^{4+} ions have nominally a $5f^2$ configuration, i.e. an even number of electrons, which does not allow for a Kramers degenerate ground state because of integer total spin. However, in the cubic crystal symmetry of these materials the orbital degeneracy may be not completely lifted, so that there can be an approximate twofold degeneracy of the U^{4+} ground state, corresponding to two different orientations of the electrical quadrupole moment of the 5f orbital in the lattice (quadrupolar Kondo effect) [12, 13]. This degree of freedom may be flipped by scattering of conduction electrons (which in the cubic symmetry also have a twofold angular momentum degeneracy). The conduction electron spin is conserved in this scattering process, leaving it as a Kramers degenerate scattering channel degree of freedom, which we will label by $\mu = 1, ..., M$, $M = 2$. Describing the orbital degree of freedom as

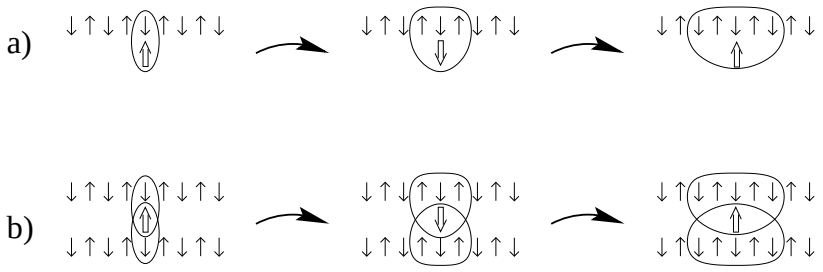

Fig. 1. Sketch of the renormalization group for a) the single–channel Kondo model (local moment compensation) and b) the two–channel Kondo model (local moment over–compensation). Small arrows denote conduction electron spins 1/2, a heavy arrow a localized spin 1/2. The curved arrows indicate successive renormalization steps.

a pseudospin 1/2, labelled by the quantum number $\sigma = 1, \ldots, N$, $N = 2$, in analogy to the magnetic Kondo effect, we arrive at the SU(2)×SU(M) symmetric Kondo model,

$$H = \sum_{\vec{k},\sigma,\mu} \varepsilon_{\vec{k}} c^{\dagger}_{\vec{k}\mu\sigma} c_{\vec{k}\mu\sigma} + J \sum_{\vec{k},\vec{k}',\sigma,\sigma',\mu} c^{\dagger}_{\vec{k}\mu\sigma} \vec{S} \cdot \vec{\tau}_{\sigma\sigma'} c_{\vec{k}\mu\sigma'}, \tag{2.2}$$

where $\vec{S}$ is the local pseudospin operator and $\vec{\tau}_{\sigma\sigma'}$ the vector of Pauli matrices. To keep the naming uniform, we will refer to the orbital degree of freedom as the (pseudo)spin or local moment, σ, in analogy to the magnetic Kondo effect, and to the physical electron spin as the channel degree of freedom, μ. In the multi–channel case, too, the conduction electrons of each channel *separately* screen the impurity moment by multiple spin scattering at temperatures below the Kondo scale T_K. However, in this case, the local moment is over–compensated, since the impurity spin can never form a singlet state with both conduction electron channels at the same time in this way, as can be seen in Fig. 1 b). As a consequence of this frustration, there is not a unique ground state, leading to a finite residual entropy [21, 22] at $T = 0$ of $S(0) = k_B \ln\sqrt{2}$ in the two–channel model. In particular, the precondition of FL theory of a 1:1 correspondence between interacting and non–interacting states is violated. As a consequence, characteristic singular temperature dependence [21, 23] of physical quantities persists for $T \lesssim T_K$ down to $T = 0$: $\chi(T) \propto -\ln(T/T_K)$, $c(T)/T \propto -\ln(T/T_K)$ and $\rho(T) - \rho(0) \propto -\sqrt{T/T_K}$. Note, however, that this behavior may be changed by any crystal field splitting of the quadrupolar non–Kramers ground state doublet.

In order to apply standard field theoretical methods to the multi–channel Kondo model it is convenient to consider it as the low–energy limiting case of

a corresponding Anderson model as discussed for the single–channel case. Here, in addition, the conservation of the channel degree of freedom has to be guaranteed. This can be implemented in an elegant way using an auxiliary boson representation to be discussed in the next section.

3. Auxiliary particle representation

As discussed above, the local level of a quantum impurity in the limit of infinitely strong local Coulomb repulsion U between electrons in the same level allows only for at most single electron occupation of the level, $n_d \leq 1$. One should note that for a realistic finite value of U the low–energy physics of the model is effectively still confined to the part of the Hilbert space without multiple occupancy. Therefore, the model Eq. (2.1) in the limit $U \to \infty$ is the generic model for the physics of quantum impurities at large U in general.

A powerful technique for implementing the projection in Hilbert space caused by a large Coulomb repulsion U is the method of auxiliary particles (slave bosons, pseudofermions) [24]. Each Fock state $|\alpha\rangle$ of the impurity is assigned a creation operator, which can be envisaged as creating the state out of a vacuum state $|\mathrm{vac}\rangle$ without any impurity level at all, $|\alpha\rangle = a_\alpha^\dagger|\mathrm{vac}\rangle$. (E.g., for a single orbital there are four such states, $|0\rangle$ (empty orbital), $|\uparrow\rangle$ or $|\downarrow\rangle$ (orbital occupied by a single electron with spin $\uparrow$ or $\downarrow$) and $|2\rangle$ (level occupied by two electrons with spin $\uparrow$ and $\downarrow$).) Due to the requirements of Fermi statistics, the creation operators $a_\alpha^\dagger$ are Fermi (Bose) operators for the states holding an odd (even) number of electrons (or vice versa). The physical state corresponds to the sector of Fock space with exactly one auxiliary particle, $\sum_\alpha n_\alpha = 1$, where $n_\alpha = a_\alpha^\dagger a_\alpha$ is the occupation number operator of particles α. Compared to alternative ways of effecting the projection, the auxiliary particle method has the advantage of making available the powerful machinery of quantum field theory, provided the constraint on the total auxiliary particle number can be incorporated in a satisfactory way.

For the quantum impurity models of the Anderson type introduced in the preceding section, only particles creating empty and singly occupied states are needed. We define N pseudofermion creation operators $f_\sigma^\dagger$ for each of the singly occupied states (labelled by $\sigma = 1, 2, \ldots, N$) and M boson creation operators $b_\mu^\dagger$ for each of the empty states created when an electron hops from the impurity into the μ-th conduction electron band (labelled by $\mu = 1, 2, \ldots, M$). In terms of these operators the Hamiltonian

of the SU(N)×SU(M) Anderson model Eq. (2.1) takes the form

$$H = \sum_{\vec{k},\sigma,\mu} \varepsilon_{\vec{k}} c^\dagger_{\vec{k}\mu\sigma} c_{\vec{k}\mu\sigma} + E_d \sum_\sigma f^\dagger_\sigma f_\sigma + V \sum_{\vec{k},\sigma,\mu} (c^\dagger_{\vec{k}\mu\sigma} b^\dagger_{\bar{\mu}} f_\sigma + h.c.) \tag{3.1}$$

In order for H to be SU(M) invariant, the slave boson multiplet $b_{\bar{\mu}}$ transforms according to the conjugate representation of the SU(M). In addition, the operator constraint

$$Q \equiv \sum_\sigma f^\dagger_\sigma f_\sigma + \sum_\mu b^\dagger_{\bar{\mu}} b_{\bar{\mu}} = 1 \tag{3.2}$$

has to be satisfied at all times. One might interpret the constraint as a statement of charge quantization, with the integer Q the conserved, quantized charge. Similar to quantum field theories with conserved charges, the charge conservation is intimately related to the existence of a local gauge symmetry. Indeed, the system defined by the Hamiltonian Eq. (3.1) is invariant under simultaneous local $U(1)$ gauge transformations $f_\sigma \to f_\sigma \mathrm{e}^{i\phi(\tau)}$, $b_{\bar{\mu}} \to b_{\bar{\mu}} \mathrm{e}^{i\phi(\tau)}$, with $\phi(\tau)$ an arbitrary time dependent phase.

3.1. Exact projection onto the physical Hilbert space

While the gauge symmetry guarantees the conservation of the quantized charge Q, it does not single out any particular Q, such as $Q = 1$. In order to effect the projection onto the sector of Fock space with $Q = 1$, one may use a procedure first proposed by Abrikosov [25]: Consider first the grand–canonical ensemble with respect to Q, defined by the statistical operator

$$\hat{\rho}_G = \frac{1}{Z_G} \mathrm{e}^{-\beta(H+\lambda Q)}, \tag{3.3}$$

where $Z_G = \mathrm{tr}[\exp\{-\beta(H+\lambda Q)\}]$ is the grand–canonical partition function with respect to Q, $-\lambda$ is the associated chemical potential, and the trace extends over the complete Fock space, including summation over Q. The expectation value of an observable $\hat{A}$ in the grand–canonical ensemble is given by

$$\langle \hat{A} \rangle_G = \mathrm{tr}[\hat{\rho}_G \hat{A}]. \tag{3.4}$$

The physical expectation value of $\hat{A}$, $\langle \hat{A} \rangle$, is to be evaluated in the canonical ensemble where $Q = 1$. It can be calculated from the grand–canonical ensemble by differentiating with respect to the fugacity $\zeta = \mathrm{e}^{-\beta\lambda}$ and taking λ to infinity [26],

$$\langle \hat{A} \rangle = \lim_{\lambda\to\infty} \frac{\frac{\partial}{\partial\zeta} \mathrm{tr}[\hat{A} e^{-\beta(H+\lambda Q)}]}{\frac{\partial}{\partial\zeta} \mathrm{tr}[e^{-\beta(H+\lambda Q)}]} = \lim_{\lambda\to\infty} \frac{\langle Q\hat{A} \rangle_G}{\langle Q \rangle_G} \ . \tag{3.5}$$

Projecting operators acting on the impurity states:— We list two important results, which follow straightforwardly from Eq. (3.5): First, the canonical partition function in the subspace $Q = 1$ is

$$\begin{aligned} Z_C &= \lim_{\lambda\to\infty} \mathrm{tr}[Qe^{-\beta(H+\lambda(Q-1))}] \\ &= \lim_{\lambda\to\infty} (e^{\beta\lambda}\langle Q\rangle_G(\lambda)) Z_{Q=0} \quad , \end{aligned} \tag{3.6}$$

where the subscripts G and C denote the grand–canonical and the canonical ($Q = 1$) expectation value, respectively. Second, the canonical $Q = 1$ expectation value of any operator $\hat{A}$ which has a zero expectation value in the $Q = 0$ subspace, $\hat{A}|Q = 0\rangle = 0$, is given by,

$$\langle \hat{A}\rangle_C = \lim_{\lambda\to\infty} \frac{\langle \hat{A}\rangle_G(\lambda)}{\langle Q\rangle_G(\lambda)} \tag{3.7}$$

Note that $\hat{A}|Q = 0\rangle = 0$ holds true for any physically observable operator acting on the impurity. Examples are the physical electron operator $d^\dagger_{\mu\sigma} = f^\dagger_\sigma b_{\bar{\mu}}$ or the local spin operator $\vec{S} = \sum_{\sigma\sigma'} \frac{1}{2} f^\dagger_\sigma \vec{\tau}_{\sigma\sigma'} f_{\sigma'}$. In this case the operator Q appearing in the numerator of Eq. (3.5) is not necessary to project away the $Q = 0$ sector. In particular, the constrained d–electron Green's function is given in terms of the grand–canonical one ($G_d(\omega, T, \lambda)$) as

$$G_d(\omega) = \lim_{\lambda\to\infty} \frac{G_d(\omega, T, \lambda)}{\langle Q\rangle_G(\lambda)} \tag{3.8}$$

In the enlarged Hilbert space ($Q = 0, 1, 2, ...$) $G_d(\omega, T, \lambda)$ may be expressed in terms of the grand–canonical pseudo–fermion and slave boson Green's functions using Wick's theorem. These auxiliary particle Green's functions, which constitute the basic building blocks of the theory, are defined in imaginary time representation as

$$\mathcal{G}_{f\sigma}(\tau_1 - \tau_2) = -\langle T\{f_\sigma(\tau_1) f^\dagger_\sigma(\tau_2)\}\rangle_G \tag{3.9a}$$

$$\mathcal{G}_{b\bar{\mu}}(\tau_1 - \tau_2) = -\langle T\{b_{\bar{\mu}}(\tau_1) b^\dagger_{\bar{\mu}}(\tau_2)\}\rangle_G \ , \tag{3.9b}$$

where T is the time ordering operator. The Fourier transforms of $\mathcal{G}_{f,b}$ may be expressed in terms of the exact self–energies $\Sigma_{f,b}$ as

$$\mathcal{G}_{f,b}(i\omega_n) = \left\{ [\mathcal{G}^0_{f,b}(i\omega_n)]^{-1} - \Sigma_{f,b}(i\omega_n) \right\}^{-1} \tag{3.10}$$

where

$$\mathcal{G}^0_{f\sigma}(i\omega_n) = (i\omega_n - E_d - \lambda)^{-1} \tag{3.11a}$$

$$\mathcal{G}^0_{b\bar{\mu}}(i\omega_n) = (i\omega_n - \lambda)^{-1} \tag{3.11b}$$

Since as a consequence of the projection procedure $\lambda \to \infty$ the energy eigenvalues of $H + \lambda Q$ scale to infinity as λQ, it is useful to shift the zero of the auxiliary particle frequency scale by λ (in the $Q = 1$ sector) and to define the "projected" Green's functions as

$$G_{f,b}(\omega) = \lim_{\lambda \to \infty} \mathcal{G}_{f,b}(\omega + \lambda) \tag{3.12}$$

Note that this does not affect the energy scale of physical quantities (like the local d electron Green's function), which is the *difference* between the the pseudo–fermion and the slave–boson energy.

Canonical expectation values of conduction electron operators:— The canonical (i.e. projected onto the $Q = 1$ subspace), local conduction electron Green function is given as

$$G_{c\mu\sigma}(i\omega_n) = \Big\{ [G^0_{c\mu\sigma}(i\omega_n)]^{-1} - \Sigma_{c\mu\sigma}(i\omega_n) \Big\}^{-1} \tag{3.13}$$

with

$$G^0_{c\mu\sigma}(i\omega_n) = \sum_{\vec{k}} G^0_{c\mu\sigma}(\vec{k}, i\omega_n) = \sum_{\vec{k}} (i\omega_n + \mu_c - \epsilon_{\vec{k}})^{-1} \ , \tag{3.14}$$

where μ_c is the chemical potential of the conduction electrons. The canonical, local c–electron self–energy, $\Sigma_{c\mu\sigma}(i\omega_n)$, cannot be obtained from the grand–canonical one by simply taking the limit $\lambda \to \infty$, since the c-electron density has a non–vanishing expectation value in the $Q = 0$ subspace. However, it follows immediately from the Anderson Hamiltonian (2.1), that the exact, canonical conduction electron t–matrix $t_{\sigma\mu}(i\omega)$, defined by $G_c = G^0_c[1 + tG^0_c]$, is is proportional to the full, projected d–electron Green's function, $t_{\mu\sigma}(i\omega) = |V|^2 G_{d\mu\sigma}$. Thus, we have as an exact relation,

$$G_{c\mu\sigma}(i\omega_n) = G^0_{c\mu\sigma}(i\omega_n) \Big[1 + |V|^2 G_{d\mu\sigma}(i\omega_n) G^0_{c\mu\sigma}(i\omega_n) \Big] \ , \tag{3.15}$$

and by comparison with Eq. (3.13) we obtain the local conduction electron self–energy respecting the constrained dynamics in the impurity orbital,

$$\Sigma_{c\mu\sigma}(i\omega_n) = \frac{|V|^2 G_{d\mu\sigma}(i\omega_n)}{1 + |V|^2 G^0_{c\mu\sigma}(i\omega_n) G_{d\mu\sigma}(i\omega_n)} \ . \tag{3.16}$$

Using phenomenological Fermi liquid theory [20] and also by means of perturbation theory to infinite order in the on–site repulsion U [27] it has been shown for the Fermi liquid case $M = 1$ of the symmetric Anderson

model ($2E_d = -U$) that the exact d–electron propagator $G_{d\sigma}(\omega)$ and the d–electron self–energy $\Sigma_{d\sigma}(\omega) \equiv \omega - G_{d\sigma}(\omega)^{-1}$ obey the following local Fermi liquid relations in the limit $\omega \to 0 - i0$, $T \to 0$,

$$\text{Luttinger theorem:} \qquad \int d\omega \; f(\omega) \frac{\partial \Sigma_{d\sigma}(\omega)}{\partial \omega} \; G_{d\sigma}(\omega) = 0 \tag{3.17}$$

$$\text{Friedel–Langreth:} \qquad \frac{1}{\pi} \mathrm{Im} G_{d\sigma}(\omega) = \frac{1}{\Gamma} \sin^2\Big(\frac{\pi n_d}{N}\Big) - c\,\Big[\Big(\frac{\omega}{T_K}\Big)^2 + \Big(\frac{\pi T}{T_K}\Big)^2\Big] \tag{3.18}$$

$$\mathrm{Im}\Sigma_{d\sigma}(\omega) = \frac{\Gamma}{\sin^2(\pi n_d/N)} + c\Big(\frac{\Gamma}{\sin^2(\pi n_d/N)}\Big)^2\Big[\Big(\frac{\omega}{T_K}\Big)^2 + \Big(\frac{\pi T}{T_K}\Big)^2\Big], \tag{3.19}$$

where c is a constant of $O(1)$. Combining Eqs. (3.16), (3.18) it follows that (for $M = 1$, away from particle hole symmetry) $\Sigma_{c\sigma}$ exhibits (in an exact theory) local Fermi liquid behavior as well, $\mathrm{Im}\Sigma_{c\sigma}(\omega - i0, T = 0) = a + b(\omega/T_K)^2$ for $\omega \to 0$. Note that this quantity is different from the grand–canonical conduction electron self–energy and has a finite imaginary part at the Fermi level.

The momentum dependent conduction electron Green's function in the presence of a single impurity is given in terms of the canonical d–electron propagator as

$$G_{c\mu\sigma}(\vec{k}, \vec{k}' \; ; \; i\omega_n) = G^0_{c\mu\sigma}(\vec{k}, i\omega_n)\Big[\delta_{\vec{k},\vec{k}'} + |V|^2 G_d(i\omega_n) G^0_{c\mu\sigma}(\vec{k}', i\omega_n)\Big] \; . \tag{3.20}$$

The latter expression is the starting point for treating a random system of many Anderson impurities [28].

3.2. Analytical properties and infrared behavior

The Green's functions $G_{f,b,c}$ have the following spectral representations

$$G_{f,b,c}(i\omega_n) = \int_{-\infty}^{\infty} d\omega' \frac{A_{f,b,c}(\omega')}{i\omega_n - \omega'} \tag{3.21}$$

with the normalization of the spectral functions $A_{f,b,c}$

$$\int_{-\infty}^{\infty} d\omega A_{f,b,c}(\omega) = 1. \tag{3.22}$$

Taking the limit $\lambda \to \infty$ has important consequences on the analytical structure of the auxiliary particle Green's functions:

(1) — It follows directly from the definitions Eqs. (3.12), (3.9), using Eqs. (3.3), (3.4), that the traces appearing in the canonical functions $G_{f,b}$ are taken purely over the $Q = 0$ sector of Fock space [1]. Thus, the backward–in–time ($\tau_1 < \tau_2$) or hole–like contribution to the auxiliary propagators in Eq. (3.9) vanishes after projection, and we have

$$G_{f\sigma}(\tau_1 - \tau_2) \;=\; -\Theta(\tau_1 - \tau_2) \lim_{\lambda\to\infty} \langle f_\sigma(\tau_1) f^\dagger_\sigma(\tau_2)\rangle_G \tag{3.23a}$$

$$G_{b\bar\mu}(\tau_1 - \tau_2) \;=\; -\Theta(\tau_1 - \tau_2) \lim_{\lambda\to\infty} \langle b_{\bar\mu}(\tau_1) b^\dagger_{\bar\mu}(\tau_2)\rangle_G \;. \tag{3.23b}$$

Consequently, their spectral functions $A_{f,b}$ have the Lehmann representation

$$A_{f\sigma}(\omega) \;=\; \sum_{m,n\geq 0} \mathrm{e}^{-\beta E^0_m} \mid \langle 1,n|f^\dagger_\sigma|0,m\rangle \mid^2 \delta(\omega - (E^1_n - E^0_m)) \tag{3.24a}$$

$$A_{b\bar\mu}(\omega) \;=\; \sum_{m,n\geq 0} \mathrm{e}^{-\beta E^0_m} \mid \langle 1,n|b^\dagger_{\bar\mu}|0,m\rangle \mid^2 \delta(\omega - (E^1_n - E^0_m)) \;, \tag{3.24b}$$

where E^Q_n are the energy eigenvalues ($E^0_0 \leq E^Q_n$ is the ground state energy) and $|Q,n\rangle$ the many–body eigenstates of H in the sector Q of Fock space. At zero temperature, A_f reduces to $A_{f\sigma}(\omega) = \sum_{n\geq 0} \mid \langle 1,n|f^\dagger_\sigma|0,0\rangle \mid^2 \delta(\omega - (E^1_n - E^0_m))$ and similar for A_b. It is seen that the $A_{f,b}$ have threshold behavior at $\omega = E_0 \equiv E^1_0 - E^0_0$, with $A_{f,b}(\omega) \equiv 0$ for $\omega < E_0$, $T = 0$. The vanishing imaginary part at frequencies $\omega < 0$ may be shown to be a general property of all quantities involving slave particle operators, e.g. also of auxiliary particle self–energies and vertex functions.

(2) — As will be seen in section 4.2 (Eq. (4.2d)), physical expectation values not only involve the particle–like auxiliary propagators Eq. (3.23) but also hole–like contributions. It is, therefore, useful to define the "anti–fermion" and "anti–boson" propagators (in imaginary time representation)

$$G^-_{f\sigma}(\tau_1 - \tau_2) \;=\; \Theta(\tau_2 - \tau_1) \lim_{\lambda\to\infty} \langle f^\dagger_\sigma(\tau_2) f_\sigma(\tau_1)\rangle_G \tag{3.25a}$$

$$G^-_{b\bar\mu}(\tau_1 - \tau_2) \;=\; \Theta(\tau_2 - \tau_1) \lim_{\lambda\to\infty} \langle b^\dagger_{\bar\mu}(\tau_2) b_{\bar\mu}(\tau_1)\rangle_G \;, \tag{3.25b}$$

whose spectral functions have the Lehmann representations

$$A^-_{f\sigma}(\omega) \;=\; \sum_{m,n\geq 0} \mathrm{e}^{-\beta E^1_m} \mid \langle 0,n|f_\sigma|1,m\rangle \mid^2 \delta(\omega - (E^0_n - E^1_m)) \tag{3.26a}$$

[1] This means that the auxiliary particle propagators are *not* calculated in the canonical ($Q = 1$) ensemble. The projection onto the $Q = 1$ sector of Fock space is achieved only when they are combined to calculate expectation values of physically observable operators like $G_{d\sigma}$, $\langle \vec{S}\rangle$ etc. The latter can be seen explicitly, e.g., from Eq. (4.2d), 2nd equality.

$$A^-_{b\bar{\mu}}(\omega) \;=\; \sum_{m,n\geq 0} \mathrm{e}^{-\beta E^1_m} \mid \langle 0,n|b_{\bar{\mu}}|1,m\rangle \mid^2 \delta(\omega - (E^0_n - E^1_m)) \;. \quad (3.26b)$$

E^1_0 is the ground state energy in the $Q = 1$ sector. The expressions (3.24) and (3.26) immediately imply a relation between $A_{f,b}$ and $A^-_{f,b}$,

$$A^-_{f,b}(\omega) = \mathrm{e}^{-\beta\omega} A_{f,b}(\omega) \;. \quad (3.27)$$

(3) — The property of only forward–in–time propagation (Eqs. (3.23), (3.24)) means that the auxiliary particle propagators $G_{f,b}$ are formally identical to the core propagators of the well–known X–ray threshold problem [29]–[31]. Thus, the knowledge of the infrared behavior of the latter may be directly applied to the former. In particular, the spectral functions are found (see below) to diverge at the threshold E_0 in a power law fashion (infrared singularity)

$$A_{f,b}(\omega) \sim |\omega - E_0|^{-\alpha_{f,b}} \theta(\omega - E_0) \quad (3.28)$$

due to a diverging number of particle–hole excitation processes in the conduction electron sea as $\omega \to E_o$.

For the single channel case ($M = 1$), i.e. the usual Kondo or mixed valence problem, the exponents α_f and α_b can be found analytically from the following chain of arguments: Anticipating that in this case the impurity spin is completely screened by the conduction electrons at temperature $T = 0$, leaving a pure-potential scattering center, the ground state $|1,0\rangle$ is a slater determinant of one–particle scattering states, characterized by scattering phase shifts η_σ in the s–wave channel (assuming for simplicity a momentum independent hybridization matrix element V). To calculate the fermion spectral function $A_{f\sigma}(\omega)$ at $T = 0$ from Eq. (3.24a), one needs to evaluate $\langle 1,n \mid f^\dagger_\sigma \mid 0,0\rangle$, which is just the overlap of two slater determinants, an eigenstate of the fully interacting Kondo system, $|1,n\rangle$, on the one hand, and the ground state of the conduction electron system in the absence of the impurity combined with the decoupled impurity level occupied by an electron with spin σ, $f^\dagger_\sigma|0,0\rangle$, on the other hand. As shown by Anderson [29], the overlap of the two ground state slater determinants, $\langle 1,0 \mid f^\dagger_\sigma \mid 0,0\rangle$, tends to zero in the thermodynamic limit (orthogonality catastrophe). Analogous relations hold for the boson spectral function $A_b(\omega)$. As a result, the long–time relaxation into the interacting ground state is inhibited, leading to the infrared power law divergence of the spectral functions, Eq. (3.28).

The X–ray threshold exponents can be expressed in terms of the scattering phase shifts at the Fermi level by the exact relation [32]

$$\alpha_{f,b} \;=\; 1 - \sum_{\sigma'} \Big(\frac{\eta_{f,b\,\sigma'}}{\pi}\Big)^2 \;. \quad (3.29a)$$

Here the $\eta_{f\sigma'}$ ($\eta_{b\sigma'}$) are the scattering phase shifts of the single–particle wave functions in channel σ' of the fully interacting ground state $|1,0\rangle$, relative to the wave functions of the free state $f_\sigma^\dagger|0,0\rangle$ ($b^\dagger|0,0\rangle$). Via the Friedel sum rule, the scattering phase shifts are, in turn, related to the change $\Delta n_{c\sigma'}$ of the average number of conduction electrons per scattering channel σ' due to the presence of the impurity: $\eta_{f,b\,\sigma'} = \pi\Delta n_{c\sigma'}$. Obviously, $\Delta n_{c\sigma'}$ is equal and opposite in sign to the difference of the average impurity occupation numbers of the states $|1,0\rangle$ and $f_\sigma^\dagger|0,0\rangle$ ($b^\dagger|0,0\rangle$). Thus, in the pseudofermion propagator $G_{f\sigma}$ we have the phase shifts,

$$\eta_{f\sigma'} = -\pi\Big(\frac{n_d}{N} - \delta_{\sigma\sigma'}\Big) \tag{3.30a}$$

and in the slave boson propagator G_b,

$$\eta_b = -\pi\frac{n_d}{N}\ , \tag{3.31a}$$

where n_d denotes the total occupation number of the impurity level in the interacting ground state. (The term $\delta_{\sigma\sigma'}$ in $\eta_{f\,\sigma'}$ appears because $f_\sigma^\dagger|0,0\rangle$ has impurity occupation number 1.) For example, in the Kondo limit $n_d \to 1$ and for a spin 1/2 impurity ($N = 2$) this leads to resonance scattering, $\eta_{f,b\,\sigma'} = \pi/2$. As a result, one finds [33] for the threshold exponents

$$\alpha_f \ = \ \frac{2n_d - n_d^2}{N} \tag{3.32a}$$

$$\alpha_b \ = \ 1 - \frac{n_d^2}{N} \tag{3.32b}$$

These results have been found independently from Wilson's numerical renormalization group approach [34, 35] and using the Bethe ansatz solution and boundary conformal field theory [36]. It is interesting to note that (i) the exponents depend on the level occupancy n_d (in the Kondo limit $n_d \to 1$, $\alpha_f = 1/N$ and $\alpha_b = 1 - 1/N$, whereas in the opposite, empty orbital, limit $n_d \to 0$, $\alpha_f \to 0$ and $\alpha_b \to 1$) (ii) the sum of the exponents $\alpha_f + \alpha_b = 1 + 2\frac{n_d(1-n_d)}{N} \geq 1$.

We stress that the above derivation of the infrared exponents $\alpha_{f,b}$ holds true only if the impurity complex acts as a pure potential scattering center at $T = 0$. This is equivalent to the statement that the conduction electrons behave locally, i.e. at the impurity site, like a Fermi liquid. Conversely, in the multi–channel (non–FL) case, $N \geq 2$, $M \geq N$, the exponents have been found from a conformal field theory solution [23] of the problem in the Kondo limit to be $\alpha_f = M/(M+N)$, $\alpha_b = N/(M+N)$, which differ from the FL values. Thus, one may infer from the values of $\alpha_{f,b}$ as a function of n_d, whether or not the system is in a local Fermi liquid state.

4. Mean field and non-crossing approximations

For physical situations of interest, the $s-d$ hybridization of the Anderson model (2.1) is much smaller than the conduction band width, $\mathcal{N}(0)V \ll 1$, where $\mathcal{N}(0) = 1/D$ is the local conduction electron density of states at the Fermi level. This suggests a perturbation expansion in $\mathcal{N}(0)V$. A straightforward expansion in terms of bare Green's functions is not adequate, as it would not allow to capture the physics of the Kondo screened state, or else the infrared divergencies of the auxiliary particle spectral functions discussed in the last section. In the framework of the slave boson representation, two types of nonperturbative approaches have been developed. The first one is mean field theory for both the slave boson amplitude $\langle b \rangle$ and the constraint ($\langle Q \rangle = 1$ rather than $Q = 1$). The second one is resummation of the perturbation theory to infinite order.

4.1. Slave boson mean field theory

Slave boson mean field theory is based on the assumption that the slave bosons condense at low temperatures such that $\langle b_{\bar{\mu}} \rangle \neq 0$. Replacing the operator $b_{\bar{\mu}}$ in $H+\lambda Q$ by $\langle b_{\bar{\mu}} \rangle$ (see Ref. [37]), where λ is a Lagrange multiplier to be adjusted such that $\langle Q \rangle = 1$, one arrives at a resonance level model for the pseudofermions. The position of the resonance, $E_d + \lambda$, is found to be given by the Kondo temperature T_K, and is thus close to the Fermi energy. The resonance generates the low energy scale T_K, and leads to local Fermi liquid behavior. While this is qualitatively correct in the single–channel case, it is in blatant disagreement with the exactly known behavior in the multi–channel case. The mean field theory can be shown to be exact for $M = 1$ in the limit $N \to \infty$ for a model in which the constraint is softened to be $Q = N/2$. However, for finite N the breaking of the local gauge symmetry, which would be implied by the condensation of the slave boson field, is forbidden by Elitzur's theorem [38]. It is known that for finite N the fluctuations in the phase of the complex expectation value $\langle b_{\bar{\mu}} \rangle$ are divergent and lead to the suppression of $\langle b_{\bar{\mu}} \rangle$ to zero (see also [39]–[41]). This is true in the cartesian gauge, whereas in the radial gauge the phase fluctuations may be shown to cancel at least in lowest order. It has not been possible to connect the mean field solution, an apparently reasonable description at low temperatures and for $M = 1$, to the high temperature behavior ($T \gg T_K$), dominated by logarithmic temperature dependence, in a continuous way [37]. Therefore, it seems that the slave boson mean field solution does not offer a good starting point even for only a qualitatively correct description of quantum impurity models.

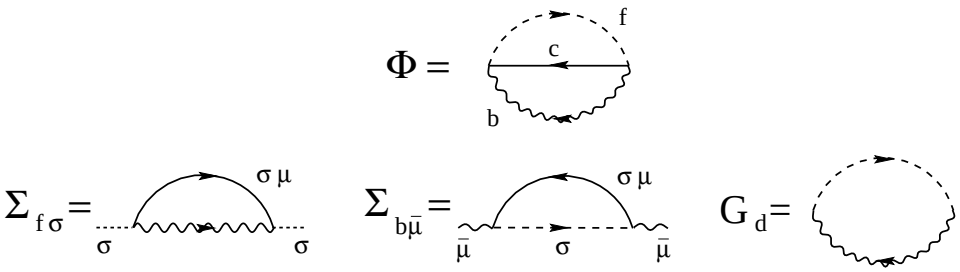

Fig. 2. Diagrammatic representation of the generating functional Φ of the NCA. Also shown are the pseudoparticle self–energies and the local electron Green's function derived from Φ, Eqs. (19)–(21). Throughout this article, dashed, wavy and solid lines represent fermion, boson, and conduction electron lines, respectively. In the diagram for $\Sigma_{f\sigma}$ the spin labels are shown explicitly to demonstrate that there are no coherent spin fluctuations taken into account.

4.2. 1/N expansion vs. self–consistent formulation

The critical judgement of mean field theory is corroborated by the results of a straightforward $1/N$-expansion in the single channel case, keeping the exact constraint, and not allowing for a finite bose field expectation value [42]. Within this scheme the exact behavior of the thermodynamic quantities (known from the Bethe ansatz solution) at low temperatures as well as high temperatures is recovered to the considered order in $1/N$. Also, the exact auxiliary particle exponents $\alpha_{f,b}$ are reproduced in order $1/N$, using a plausible exponentiation scheme [43].

In addition, dynamical quantities like the d-electron spectral function and transport coefficients can be calculated exactly to a desired order in $1/N$, within this approach. However, as clear-cut and economical this method may be, it does have serious limitations. For once, the experimentally most relevant case of $N = 2$ or somewhat larger is not accessible in $1/N$ expansion. Secondly, non-Fermi liquid behavior, being necessarily non-perturbative in $1/N$, cannot be dealt with in a controlled way on the basis of a $1/N$-expansion. To access these latter two regimes, a new approach non-perturbative in $1/N$ is necessary.

We conjecture that this new approach is gauge invariant many-body theory of pseudofermions and slave bosons. As long as gauge symmetry violating objects such as Bose field expectation values or fermion pair correlation functions do not appear in the theory, gauge invariance of physical quantities can be guaranteed in suitably chosen approximations by the proper match of pseudofermion and slave boson properties, without introducing an additional gauge field. This requires the use of conserving approxima-

tions [44], derived from a Luttinger-Ward functional Φ. Φ consists of all vacuum skeleton diagrams built out of fully renormalized Green's functions $G_{b,f,c}$ and the bare vertex V. The self–energies $\Sigma_{b,f,c}$ are obtained by taking the functional derivative of Φ with respect to the corresponding Green's function (cutting the Green's function line in each diagram in all possible ways),

$$\Sigma_{b,f,c} = \delta\Phi/\delta G_{b,f,c}. \tag{4.1}$$

Irreducible vertex functions, figuring as integral kernels in two-particle Bethe-Salpeter equations, are generated by second order derivatives of Φ.

The choice of diagrams for Φ defines a given approximation. It should be dictated by the dominant physical processes and by expansion in a small parameter, if available. As noted before, in the present context, we may take the hybridization V to be a small quantity (dimensionless parameter $N_o V$). This suggests to start with the lowest order (in V) diagram of Φ, which is second order (see Fig. 2). The self–energies generated from this obey after analytic continuation to real frequencies ($i\omega \to \omega - i0$) and projection the following equations of self–consistent second order perturbation theory

$$\Sigma^{(NCA)}_{f\sigma}(\omega - i0) \;=\; \Gamma \sum_{\mu} \int \frac{d\varepsilon}{\pi}\, [1 - f(\varepsilon)] A^0_{c\mu\sigma}(\varepsilon) G_{b\bar{\mu}}(\omega - \varepsilon - i0) \tag{4.2a}$$

$$\Sigma^{(NCA)}_{b\bar{\mu}}(\omega - i0) \;=\; \Gamma \sum_{\sigma} \int \frac{d\varepsilon}{\pi}\, f(\varepsilon) A^0_{c\mu\sigma}(\varepsilon) G_{f\sigma}(\omega + \varepsilon - i0) \tag{4.2b}$$

$$\begin{aligned} G^{(NCA)}_{d\mu\sigma}(\omega - i0) \;&=\; \int d\varepsilon\, \mathrm{e}^{-\beta\varepsilon} [G_{f\sigma}(\omega + \varepsilon - i0) A_{b\bar{\mu}}(\varepsilon) \\ &\qquad - A_{f\sigma}(\varepsilon) G_{b\bar{\mu}}(\varepsilon - \omega + i0)] \qquad (4.2c) \\ &=\; \int d\varepsilon\, [G_{f\sigma}(\omega + \varepsilon - i0) A^-_{b\bar{\mu}}(\varepsilon) - A^-_{f\sigma}(\varepsilon) G_{b\bar{\mu}}(\varepsilon - \omega + i0)]\,, \end{aligned}$$

where $A^0_{c\mu\sigma} = \frac{1}{\pi}\,\mathrm{Im} G^0_{c\mu\sigma}/\mathcal{N}(0)$ is the (free) conduction electron density of states per spin and channel, normalized to the density of states at the Fermi level $\mathcal{N}(0)$, and $f(\varepsilon) = 1/(\exp(\beta\varepsilon)+1)$ denotes the Fermi distribution function. Together with the expressions (3.10), (3.11) for the Green's functions, Eqs. (4.2a)–(4.2d) form a set of self–consistent equations for $\Sigma_{b,f,c}$, comprised of all diagrams without any crossing propagator lines and are, thus, known as the "non–crossing approximation", in short NCA [45, 46].

At zero temperature and for low frequencies Eqs. (4.2a) and (4.2b) may be converted into a set of linear differential equations for G_f and G_b [47], which allow to find the infrared exponents as $\alpha_f = \frac{M}{M+N}$; $\alpha_b = \frac{N}{M+N}$, independent of n_d. For the single channel case these exponents do not agree with the exact exponents derived in section 3. This indicates that the NCA is not capable of recovering the local Fermi liquid behavior for

$M = 1$. A numerical evaluation of the d-electron Green's function, which is given by the local self–energy Σ_c divided by V^2 and hence is given by the boson–fermion bubble within NCA (Fig. 2), shows indeed a spurious singularity at the Fermi energy [48]. The NCA performs somewhat better in the multi–channel case, where the exponents α_f and α_b yield the correct non–Fermi liquid exponents of physical quantities as known from the Bethe ansatz solution [19] and conformal field theory [23]. However, the specific heat and the residual entropy are not given correctly in NCA. Also, the limiting low temperature scaling laws for the thermodynamic quantities are attained only at temperatures substantially below T_K, in disagreement with the exact Bethe ansatz solution.

4.3. Low–temperature evaluation of the self–consistency equations

In order to enter the asymptotic power law regime of the auxiliary spectral functions the self–consistent scheme, in particular the NCA, must be evaluated for temperatures several orders of magnitude below T_K, the low temperature scale of the model. The equations are solved numerically by iteration. In the following we describe the two main procedures to make the diagrammatic auxiliary particle technique suitable for the lowest temperatures.

The grand–canonical expectation value of the auxiliary particle number appearing in Eq. (3.8) is given in terms of the grand–canonical (unprojected) auxiliary particle spectral functions $\mathcal{A}_{f,b}(\omega,\lambda)$ by,

$$\langle Q\rangle_G(\lambda) = \int d\omega \Big[f(\omega) \sum_\sigma \mathcal{A}_{f\sigma}(\omega,\lambda) + b(\omega) \sum_\mu \mathcal{A}_{b\bar{\mu}}(\omega,\lambda) \Big] \tag{4.3}$$

where $f(\omega)$, $b(\omega)$ are the Fermi and Bose distribution functions, respectively. Substituting this into the expression (3.6) for the canonical partition function we obtain after carrying out the transformation $\omega \to \omega + \lambda$, and taking the limit $\lambda \to \infty$

$$\begin{aligned} e^{-\beta F_{imp}(T)} &\equiv \frac{Z_C}{Z_{Q=0}} = \lim_{\lambda\to\infty} e^{\beta\lambda} \langle Q\rangle_G(\lambda) \\ &= \int d\omega e^{-\beta\omega} \Big[\sum_\sigma A_{f\sigma}(\omega) + \sum_\mu A_{b\bar{\mu}}(\omega) \Big] \, . \end{aligned} \tag{4.4}$$

By definition $F_{imp} = -\frac{1}{\beta}\ln(Z_C/Z_{Q=0})$ is the impurity contribution to the Free energy.

The numerical evaluation of expectation values like $\langle Q\rangle_G(\lambda\to\infty)$ (Eq. (4.4)) or $G_{d\mu\sigma}(\omega,\lambda\to\infty)$ (Eq. (4.2d)) is non–trivial, (1) because at $T = 0$

the auxiliary spectral functions $A_{f,b}(\omega, T)$ are divergent at the threshold frequency E_0, where the exact position of E_0 is a priori not known, and (2) because the Boltzmann factors $e^{-\beta\omega}$ diverge strongly for $\omega < 0$. Therefore, we apply the following transformations:

(1) Before performing the projection $\omega \to \omega + \lambda$, $\lambda \to \infty$ we re–define the frequency scale of all auxiliary particle functions $A_{f,b}$ according to $\omega \to \omega+\lambda_0$, where λ_0 is a finite parameter. In each iteration λ_0 is then determined such that

$$\int d\omega e^{-\beta\omega} \Big[\sum_{\sigma} A_{f\sigma}(\omega) + \sum_{\mu} A_{b\bar{\mu}}(\omega) \Big] = 1 \tag{4.5}$$

where $A_{f,b}(\omega) = \lim_{\lambda\to\infty} A_{f,b}(\omega+\lambda_0, \lambda)$ is now an auxiliary spectral function with the new reference energy. It is seen by comparison with Eq. (4.4) that $\lambda_0(T) = F_{imp}(T) = F_{Q=1}(T) - F_{Q=0}(T)$, i.e. λ_0 is the chemical potential for the auxiliary particle number Q, or equivalently the impurity contribution to the Free energy. The difference of the Free energies becomes equal to the threshold energy $E_0 = E^{GS}_{Q=1} - E^{GS}_{Q=0}$ at $T = 0$. More importantly, however, the above way of determining a "threshold" is less *ad hoc* than, for example, defining it by a maximum in some function appearing in the NCA equations. It is also seen from Eq. (4.5) that this procedure defines the frequency scale of the auxiliary particles such that the $T = 0$ threshold divergence of the spectral functions is at the *fixed* frequency $\omega = 0$. This substantially increases the precision as well as the speed of numerical evaluations. Eq. (3.8) for the projected d–electron Green's function becomes

$$G_d(\omega) = \lim_{\lambda\to\infty} e^{\beta\lambda} G_d(\omega, T, \lambda). \tag{4.6}$$

(2) The divergence of the Boltzmann factors implies that the self–consistent solutions for $A_{f,b}(\omega)$ vanish exponentially $\sim e^{\beta\omega}$ for negative frequencies, confirming their threshold behavior. It is convenient, not to formulate the self–consistent equations in terms of $A_{f,b}$ like in earlier evaluations [49], but to define new functions $\tilde{A}_{f,b}(\omega)$ and $\mathrm{Im}\tilde{\Sigma}_{f,b}(\omega)$ such that

$$A_{f,b}(\omega) \;=\; f(-\omega)\; \tilde{A}_{f,b}(\omega) \tag{4.7}$$

$$\mathrm{Im}\Sigma_{f,b}(\omega) \;=\; f(-\omega)\; \mathrm{Im}\tilde{\Sigma}_{f,b}(\omega). \tag{4.8}$$

After fixing the chemical potential λ_0 and performing the projection onto the physical subspace, the canonical partition function (Eq. (3.6)) behaves as $\lim_{\lambda\to\infty} e^{\beta(\lambda-\lambda_0)}\; Z_C(T) = 1$. In this way all exponential divergencies are absorbed by one single function for each particle species. The NCA equations in terms of these functions are free of divergencies of the statistical

factors and read

$$\mathrm{Im}\tilde{\Sigma}_{f\sigma}(\omega - i0) = \Gamma \sum_{\mu} \int d\varepsilon \, \frac{f(-\varepsilon)(1 - f(\omega - \varepsilon))}{1 - f(\omega)} A^0_{c\mu\sigma}(\varepsilon) \tilde{A}_{b\bar{\mu}}(\omega - \varepsilon) \quad (4.9)$$

$$\mathrm{Im}\tilde{\Sigma}_{b\bar{\mu}}(\omega - i0) = \Gamma \sum_{\sigma} \int d\varepsilon \, \frac{f(\varepsilon)(1 - f(\omega + \varepsilon))}{1 - f(\omega)} A^0_{c\mu\sigma}(\varepsilon) \tilde{A}_{f\sigma}(\omega + \varepsilon) \quad (4.10)$$

$$\langle Q \rangle(\lambda_0, \lambda \to \infty) = \int d\omega f(\omega) \Big[\sum_{\sigma} \tilde{A}_{f\sigma}(\omega) + \sum_{\mu} \tilde{A}_{b\bar{\mu}}(\omega) \Big] = 1 \quad (4.11)$$

$$\mathrm{Im}G_{d\sigma}(\omega - i0) = \int d\varepsilon [f(\varepsilon + \omega) f(-\varepsilon) + f(-\varepsilon - \omega) f(\varepsilon)] \tilde{A}_{f\sigma}(\varepsilon + \omega) \tilde{A}_b(\varepsilon). \quad (4.12)$$

The real parts of the self–energies Σ_f, Σ_b are determined from $\mathrm{Im}\Sigma_f$, $\mathrm{Im}\Sigma_b$ through a Kramers–Kroenig relation, and the auxiliary functions $\tilde{A}_{f\sigma}(\omega) = \frac{1}{\pi}\mathrm{Im}\tilde{\Sigma}_{f\sigma}(\omega - i0)/[(\omega + \lambda_0 - i0 - E_d - \mathrm{Re}\Sigma_{f\sigma}(\omega - i0))^2 + \mathrm{Im}\Sigma_{f\sigma}(\omega - i0)^2]$, $\tilde{A}_{b\bar{\mu}}(\omega) = \frac{1}{\pi}\mathrm{Im}\tilde{\Sigma}_{b\bar{\mu}}(\omega - i0)/[(\omega + \lambda_0 - i0 - \mathrm{Re}\Sigma_{b\bar{\mu}}(\omega - i0))^2 + \mathrm{Im}\Sigma_{b\bar{\mu}}(\omega - i0)^2]$, thus closing the above set of equations.

The method described above allows to solve the NCA equations effectively for temperatures down to typically $T = 10^{-4} T_K$. It may be shown that the same procedure can also be applied to self–consistently compute vertex corrections beyond the NCA (see section 5).

5. Conserving T-matrix approximation

5.1. Dominant contributions at low energy

In order to eliminate the shortcomings of the NCA mentioned above, the guiding principle should be to find contributions to the vertex functions which renormalize the auxiliary particle threshold exponents to their correct values, since this is a necessary condition for the description of FL and non–FL behavior, as discussed in section 3. Furthermore, it is instructive to realize that in NCA any coherent spin flip and charge transfer processes are neglected, as can be seen explicitly from Eqs. (4.2a), (4.2b) or from Fig. 2. These processes are known to be responsible for the quantum coherent collective behavior of the Anderson impurity complex below T_K. The existence of collective excitations in general is reflected in a singular behavior of the corresponding two–particle vertex functions. In view of the tendency of Kondo systems to form a collective spin singlet state, we are here interested in the spin singlet channel of the pseudofermion–conduction electron vertex function and in the slave boson–conduction electron vertex function. It may

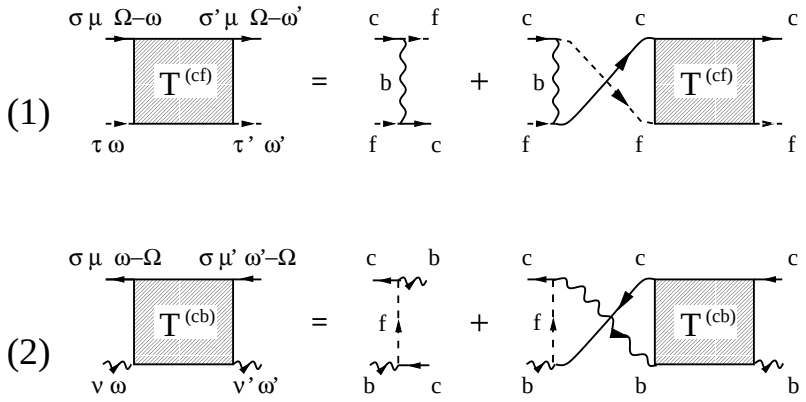

Fig. 3. Diagrammatic representation of the Bethe–Salpeter equation for (1) the conduction electron–pseudofermion T-matrix $T^{(cf)}$, Eq. (5.1), and (2) the conduction electron–slave boson T-matrix $T^{(cb)}$, Eq. (5.2). $T^{(cb)}$ is obtained from $T^{(cf)}$ by interchanging $f \leftrightarrow b$ and $c \leftrightarrow c^\dagger$.

be shown by power counting arguments (compare appendix A) that there are no corrections to the NCA exponents in any finite order of perturbation theory [50]. Thus, we are led to search for singularities in the aforementioned vertex functions arising from an infinite resummation of terms. From the preceding discussion it is natural to perform a partial resummation of those terms which, at each order in the hybridization V, contain the maximum number of spin flip or charge fluctuation processes, respectively. This amounts to calculating the conduction electron–pseudofermion vertex function in the "ladder" approximation definied in Fig. 3, where the irreducible vertex is given by $V^2 G_b$. In analogy to similar resummations for an interacting one–component Fermi system, we call the total c–f vertex function T–matrix $T^{(cf)}$. The Bethe–Salpeter equation for $T^{(cf)}$ reads (Fig. 3 (1)),

$$\begin{aligned} T^{(cf)\,\mu}_{\sigma\tau,\sigma'\tau'}(i\omega_n, i\omega_n', i\Omega_n) = &+ V^2 G_{b\bar{\mu}}(i\omega_n + i\omega_n' - i\Omega_n)\delta_{\sigma\tau'}\delta_{\tau\sigma'} \\ &- V^2 T \sum_{\omega_n''} G_{b\bar{\mu}}(i\omega_n + i\omega_n'' - i\Omega_n) \times \\ &G_{f\sigma}(i\omega_n'')\; G^0_{c\mu\tau}(i\Omega_n - i\omega_n'')\; T^{(cf)\,\mu}_{\tau\sigma,\sigma'\tau'}(i\omega_n'', i\omega_n', i\Omega_n). \end{aligned} \tag{5.1}$$

A similar integral equation holds for the charge fluctuation T–matrix $T^{(cb)}$ (Fig. 3 (2)).

$$\begin{aligned} T^{(cb)\,\sigma}_{\mu\nu,\mu'\nu'}(i\omega_n, i\omega_n', i\Omega_n) = &+ V^2 G_{f\sigma}(+i\omega_n + i\omega_n' - i\Omega_n)\delta_{\mu\nu'}\delta_{\nu\mu'} \\ &- V^2 T \sum_{\omega_n''} G_{f\sigma}(i\omega_n + i\omega_n'' - i\Omega_n) \times \end{aligned} \tag{5.2}$$

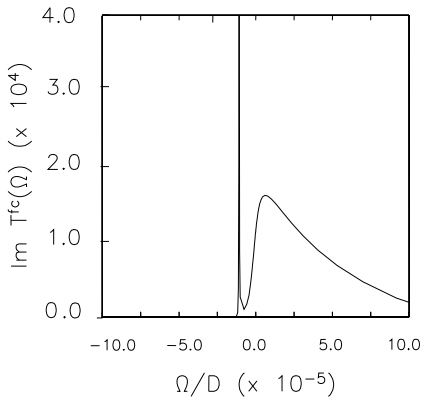

Fig. 4. Imaginary part of the conduction electron–pseudofermion T–matrix $T^{(cf)}$ as a function of the COM frequency Ω for the single–channel case $M = 1$, $N = 2$, evaluated by inserting NCA solutions for the intermediate state propagators ($E_d = -0.67D$, $\Gamma = 0.15D$, $T = 4 \cdot 10^{-3} T_K$). The contribution from the pole positioned at a negative frequency $\Omega = \Omega_{cf} \simeq -T_K$ (compare text) is clearly seen.

$$G_{b\bar{\mu}}(i\omega_n'')\; G^0_{c\nu\sigma}(-i\omega_n'' - i\Omega_n)\; T^{(cb)\;\sigma}_{\nu\mu,\mu'\nu'}(i\omega_n'', i\omega_n', i\Omega_n).$$

In the above Bethe–Salpeter equations σ, τ, σ', τ' represent spin and μ, ν, μ', ν' channel indices. Inserting NCA Green's functions for the intermediate state propagators of Eq. (5.1) and solving it numerically, we find at low temperatures and in the Kondo regime ($n_d \gtrsim 0.7$) a pole of $T^{(cf)}$ in the singlet channel (see appendix A) as a function of the center–of–mass (COM) frequency Ω, at a frequency which scales with the Kondo temperature, $\Omega = \Omega_{cf} \simeq -T_K$. This is shown in Fig. 4. The threshold behavior of the imaginary part of $T^{(cf)}$ as a function of Ω with vanishing spectral weight at negative frequencies and temperature $T = 0$ is clearly seen. In addition, a very sharp structure appears, whose broadening is found to vanish as the temperature tends to zero, indicative of a pole in $T^{(cf)}$ at the *real* frequency Ω_{cf}, i.e. the tendency to form a collective singlet state between the conduction electrons and the localized spin. Similarly, the corresponding T-matrix $T^{(cb)}$ in the conduction electron–slave boson channel, evaluated within the analogous approximation, develops a pole at negative values of Ω in the empty orbital regime ($n_d \lesssim 0.3$). In the mixed valence regime ($n_d \simeq 0.5$) the poles in both $T^{(cf)}$ and $T^{(cb)}$ coexist. The appearance of poles in the two–particle vertex functions $T^{(cf)}$ and $T^{(cb)}$, which signals the formation of collective states, may be expected to influence the behavior of the system in a major way.

5.2. Self–consistent formulation: CTMA

On the level of approximation considered so far, the description is not yet consistent: In the limit of zero temperature the spectral weight of $T^{(cf)}$ and $T^{(cb)}$ at negative frequencies Ω should be strictly zero (threshold property). Nonvanishing spectral weight at $\Omega < 0$ like a pole contribution for negative Ω in $T^{(cf)}$ or $T^{(cb)}$ would lead to a diverging contribution to the self–energy, which is unphysical. However, recall that a minimum requirement on the approximation used is the conservation of gauge symmetry. This requirement is not met when the integral kernel of the T-matrix equation is approximated by the NCA result. Rather, the approximation should be generated from a Luttinger–Ward functional. The corresponding generating functional is shown in Fig. 5. It is defined as the infinite series of all vacuum skeleton diagrams which consist of a single ring of auxiliary particle propagators, where each conduction electron line spans at most two hybridization vertices (Fig. 5). As shown in appendix A by means of a cancellation theorem, the CTMA includes, at any given loop order, all infrared singular contributions to leading and subleading order in the frequency ω. The first diagram of the infinite series of CTMA terms corresponds to NCA (Fig. 2). The diagram containing two boson lines is excluded since it is not a skeleton. Although the spirit of the present theory is different from a large N expansion, it should be noted that the sum of the Φ diagrams containing up to four boson lines includes all terms of a $1/N$ expansion up to $O(1/N^2)$ [51]. By functional differentiation with respect to the conduction electron Green's function and the pseudofermion or the slave boson propagator, respectively, the shown Φ functional generates the ladder approximations $T^{(cf)}$, $T^{(cb)}$ for the total conduction electron–pseudofermion vertex function (Fig. 3) and for the total conduction electron–slave boson vertex function. The auxiliary particle self–energies are obtained in the conserving scheme as the functional derivatives of Φ with respect to G_f or G_b, respectively (Eq. (4.1)). This defines a set of self–consistency equations, which we term conserving T–matrix approximation (CTMA), where the self–energies are given as nonlinear and nonlocal (in time) functionals of the Green's functions, while the Green's functions are in turn expressed in terms of the self–energies. The CTMA equations are derived explicitly in appendix B. The solution of these equations requires that the T–matrices have vanishing spectral weight at negative COM frequencies Ω. Indeed, the numerical evaluation shows that the poles of $T^{(cf)}$ and $T^{(cb)}$ are shifted to $\Omega = 0$ by self–consistency, where they merge with the continuous spectral weight present for $\Omega > 0$, thus renormalizing the threshold exponents of the auxiliary spectral functions.

The self–consistent solutions are obtained by first solving the linear

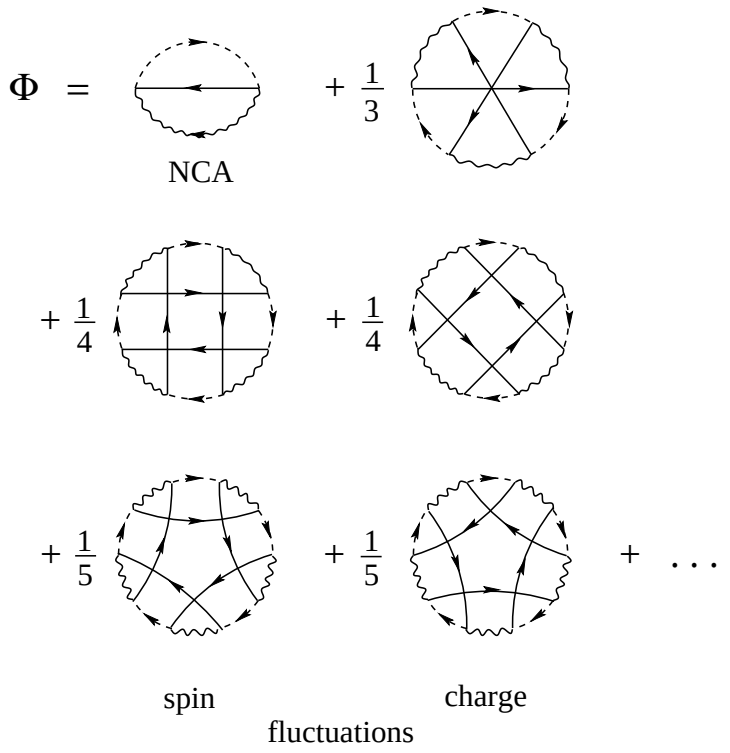

Fig. 5. Diagrammatic representation of the Luttinger–Ward functional generating the conserving T–matrix approximation (CTMA). The terms with the conduction electron lines running clockwise (labelled "spin fluctuations") generate the T–matrix $T^{(cf)}$, while the terms with the conduction electron lines running counter–clockwise (labelled "charge fluctuations") generate the T–matrix $T^{(cb)}$.

Bethe–Salpeter equations for the T–matrices by matrix inversion, computing the auxiliary particle self–energies from $T^{(cf)}$ and $T^{(cb)}$, and then constructing the fermion and boson Green's functions from the respective self–energies. This process is iterated until convergence is reached. We have obtained reliable solutions down to temperatures of the order of at least $10^{-2}T_K$ both for the single-channel and for the two-channel Anderson model. Note that $T_K \to 0$ in the Kondo limit; in the mixed valence and empty impurity regimes, significantly lower temperatures may be reached, compared to the low temperature scale of the model.

As shown in Fig. 6 (1) a), the auxiliary particle spectral functions obtained from CTMA [52] are in good agreement with the results of a numerical renormalization group (NRG) calculation [34] (zero temperature results), given the uncertainties in the NRG at higher frequencies. Typ-

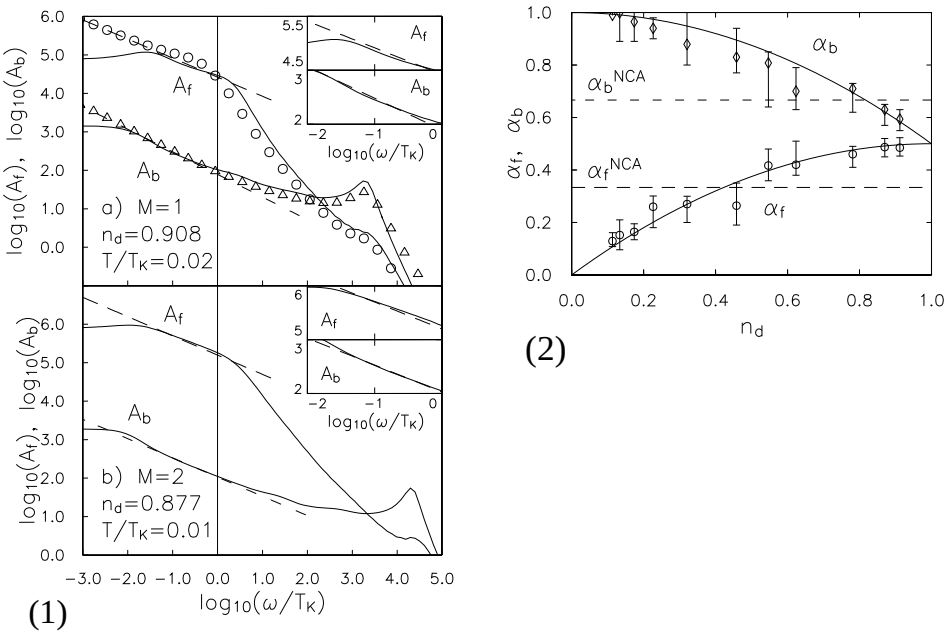

Fig. 6. (1) Pseudofermion and slave boson spectral functions A_f and A_b in the Kondo regime ($N = 2$; $E_d = -0.05$, $\Gamma = 0.01$ in units of the half–bandwidth D), for a) the single–channel ($M = 1$) and b) the multi–channel ($M = 2$) case. In a) the symbols represent the results of NRG for the same parameter set, $T = 0$. The slopes of the dashed lines indicate the exact threshold exponents as derived in section 3 for $M = 1$ and as given by conformal field theory for $M = 2$. The insets show magnified power law regions. (2) CTMA results (symbols with error bars) for the threshold exponents α_f and α_b of A_f and A_b, $N = 2$, $M = 1$. Solid lines: exact values (section 3), dashed lines: NCA results (section 4.2).

ical behavior in the Kondo regime is obtained: a broadened peak in A_b at $\omega \simeq |E_d|$, representing the hybridizing d–level and a structure in A_f at $\omega \simeq T_K$. Both functions display power law behavior at frequencies below T_K, which at finite T is cut off at the scale $\omega \simeq T$. The exponents extracted from the frequency range $T < \omega < T_K$ of our finite T results compare well with the exact result also shown (see insets of Fig. 6 (1a)). A similar analysis has been performed for a number of parameter sets spanning the complete range of d–level occupation numbers n_d. The extracted power law exponents are shown in Fig. 6 (2), together with error bars estimated from the finite frequency ranges over which the fit was made. The comparatively large error bars in the mixed valence regime arise because here spin flip and charge fluctuation processes, described by the poles in $T^{(cf)}$ and $T^{(cb)}$, respectively, are of equal importance, impeding the convergence of the nu-

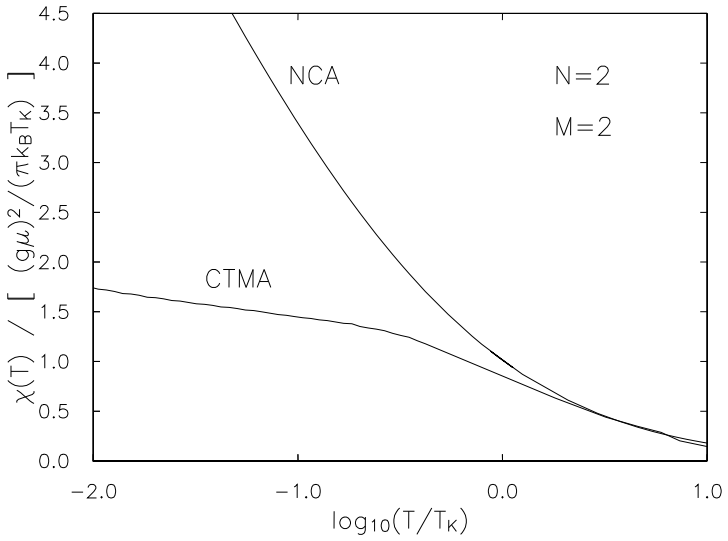

Fig. 7. Static susceptibility of the two–channel Anderson impurity model: CTMA and NCA results ($E_d = -0.8D$, $\Gamma = 0.1D$, Landé factor $g = 2$).

merical procedure. In this light, the agreement with the exact results (solid curves) is very good, the exact value lying within the error bars or very close in each case.

In the multi–channel case ($N \geq 2$, $M \geq N$) NCA has been shown [50] to reproduce asymptotically the correct threshold exponents, $\alpha_f = M/(M+N)$, $\alpha_b = N/(M+N)$, in the Kondo limit. Calculating the T–matrices using NCA Green's functions (as discussed in the single–channel case) we find again a pole in the singlet channel of $T^{(cf)}$. However, in this case the CTMA does not renormalize the NCA exponents in the Kondo limit of the two–channel model, i.e. the threshold exponents obtained from the CTMA solutions are very close to the exact ones, $\alpha_f = 1/2$, $\alpha_b = 1/2$, as shown in Fig. 6 (1) b).

The agreement of the CTMA exponents with their exact values in the Kondo, mixed valence and empty impurity regimes of the single–channel model and in the Kondo regime of the two–channel model may be taken as evidence that the T–matrix approximation correctly describes both the FL and the non–FL regimes of the SU(N)×SU(M) Anderson model (N=2, M=1,2). Therefore, we expect the CTMA to correctly describe physically observable quantities of the SU(N)×SU(M) Anderson impurity model as well. As a check, we have calculated the static spin susceptibility χ of the two–channel Anderson model in the Kondo regime by solving the CTMA equations (see appendix B) in a finite magnetic field H coupled

to the impurity spin and taking the derivative of the magnetization $M = \frac{1}{2}g\mu_B\langle n_{f\uparrow} - n_{f\downarrow}\rangle$ with respect to H. The resulting $\chi(T) = (\partial M/\partial H)_T$ is shown in Fig. 7. It is seen that CTMA correctly reproduces the exact [19] logarithmic temperature dependence below the Kondo scale T_K. In contrast, the NCA solution recovers the logarithmic behavior only far below T_K. Other physical quantities will be calculated for the Anderson model in forthcoming work.

6. Conclusion

We have presented a novel technique to describe correlated quantum impurity systems with strong onsite repulsion, which is based on a conserving formulation of the auxiliary boson method. The conserving scheme allows to preserve the conservation of the local charge Q without taking into account time dependent fluctuations of the gauge field λ. Taking, as a result, λ as a time independent quantity represents a great simplification of this approach. As a standard diagram technique this method has the potential to be applicable to problems of correlated systems on a lattice as well, while keeping the full dynamics of the pseudofermion and slave boson fields. By including the leading infrared singular contributions (spin flip and charge fluctuation processes), this technique allows to correctly describe physical quantities, like the magnetic susceptibility, both in the Fermi and in the non–Fermi liquid regime, over the complete temperature range, including the crossover to the correlated many–body state at the lowest temperatures.

We wish to thank S. Böcker, T.A. Costi, S. Kirchner, A. Rosch, A. Ruckenstein and Th. Schauerte for stimulating discussions. S. Böcker has performed part of the numerical solutions. This work is supported by DFG through SFB 195 and by the Hochleistungsrechenzentrum Jülich through a grant of computer time on a Cray T3E parallel computer.

Appendix

A. Infrared cancellation of non–CTMA diagrams

The CTMA is not only justified on physical grounds by the inclusion of the maximum number of spin flip and charge fluctuation processes at any given order of perturbation theory, but also by an infrared cancellation of all diagrams not included in the CTMA. In the following we will prove this cancellation theorem.

(1) *Power counting.*— Each auxiliary particle loop carries a factor of

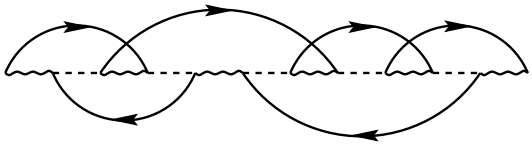

Fig. 8. Typical pseudofermion self–energy skeleton diagram of loop order $L = 6$, containing $L_{sp} = 1$ spin (or fermion) loop and $L_{ch} = 1$ channel loop.

the fugacity $\exp(-\beta\lambda)$, which vanishes upon projection onto the $Q = 1$ subspace, $\lambda \to \infty$. Therefore, an arbitrary f or b self–energy diagram consists of one single line of alternating fermion and boson propagators, with the hybridization vertices connected by conduction electron lines in any possible way, as shown in Fig. 8 (see also [45]). Such a fermion self–energy skeleton diagram of loop order L is calculated as

$$\begin{aligned}\Sigma_f^{(L)}(\omega) \;=\; & (-1)^{3L-1+L_{sp}}\; N^{L_{sp}}\; M^{L_{ch}}\; \Gamma^L \\ & \times \int \frac{d\varepsilon_1}{\pi} \ldots \frac{d\varepsilon_L}{\pi}\; f(\varepsilon_1) \ldots\; f(\varepsilon_L)\; A_c^0(s_1\varepsilon_1) \ldots A_c^0(s_L\varepsilon_L) \\ & \times G_b(\omega+\omega_1) G_f(\omega+\omega_1+\omega_1')\; \ldots \\ & \times\; \ldots\; G_b\Big(\omega + \sum_{i=1}^{k}\omega_i + \sum_{i=1}^{k-1}\omega_i'\Big)\; G_f\Big(\omega + \sum_{i=1}^{k}(\omega_i+\omega_i')\Big)\; \ldots\; G_b(\omega+\omega_L)\;,\end{aligned} \tag{A.1}$$

where $G_{f,b}$ are the *renormalized*, i.e. power law divergent auxiliary particle propagators, and L_{sp} and L_{ch} denote the number of spin (or fermion, c–f) loops and the number of channel (or c–b) loops contained in the diagram, respectively. Spin and channel indices are not shown for simplicity. Each of the auxiliary particle frequencies ω_i, ω_i' coincides with one of the integration variables ε_j, $j = 1, \ldots, L$, in such a way that energy is conserved at each hybridization vertex. This implies that the sign of the frequency carried by a c–electron line is $s_i = +$, if the c–electron line runs from right to left, and $s_i = -$, if it runs from left to right in Fig. 8. An analogous expression holds for the slave boson self–energy diagrams. By substituting $x_j = \varepsilon_j/\omega$, $j = 1, \ldots, L$ and factoring out $\omega^{-\alpha_{f,(b)}}$ from each fermion (boson) propagator, the infrared behavior of the term Eq. (A.1) is deduced as

$$\mathrm{Im}\Sigma_{f,b}^{(L)}(\omega) = C\omega^{\alpha_{f,b}+L(1-\alpha_f-\alpha_b)}, \tag{A.2}$$

where C is a finite constant. Clearly, when the NCA solutions are inserted for the propagators $G_{f,b}$, i.e. $\alpha_f + \alpha_b = 1$, their power law behavior is just reproduced by any term of the form Eq. (A.1). However, this is no longer the case for the exact propagators in the Fermi liquid regime ($M < N$),

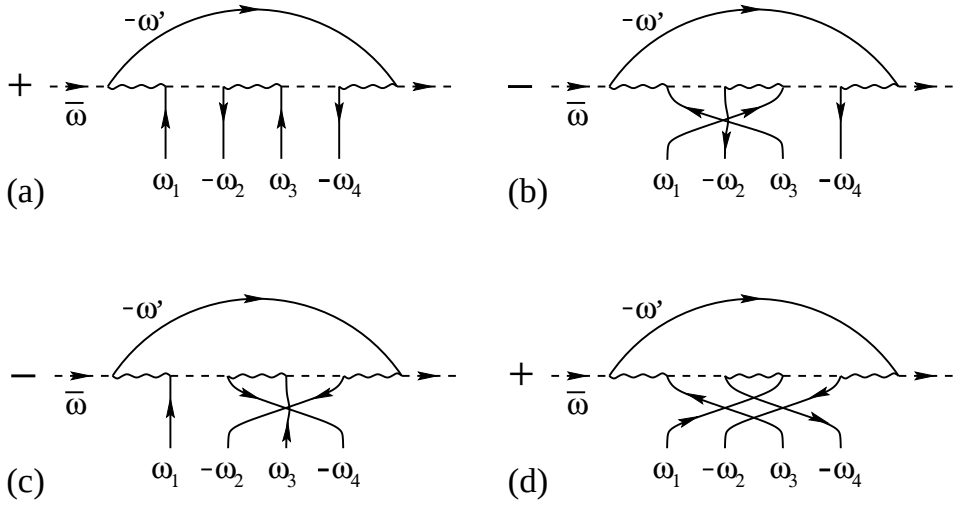

Fig. 9. Set of contributions to skeleton diagrams *not* contained in CTMA which cancel in the infrared limit to leading and subleading order in the external frequency, $\omega \to 0$.

where in general $\alpha_f + \alpha_b > 1$. Thus, the infinite resummation of terms to arbitrary loop order is unavoidable in this case.

(2) *Infrared cancellation.*— As discussed in section 5.2, the CTMA is equivalent to the self–consistent summation of all skeleton free energy diagrams, where a conduction electron line spans at most two hybridization vertices (Fig. 5). Thus, any skeleton self–energy diagram *not* included in CTMA contains at least one conduction electron "arch" which spans four (or more) vertices, with four conduction lines reaching from inside to outside of the arch as shown in Fig. 9(a). For each such diagram there exists another skeleton, which differs from Fig. 9(a) only in that the end points of two conduction lines inside the arch are interchanged (Fig. 9(b)). The corresponding permutation of fermionic operators implies a relative sign between the terms Fig. 9(a) and (b). Without loss of generality we now assume $\omega > 0$ for the external frequency of the self–energy. The leading infrared singular behavior of the term (A.1) arises from those parts of the integrations, where the arguments of the G_f, G_b are such that the divergences of all propagators lie within the integration range. This implies at least $-\omega \leq \varepsilon_j \leq 0$, $j = 1, \ldots, L$. Therefore, the terms corresponding to Fig. 9(a), (b) differ only in the frequency arguments of the Green's functions inside the arch, and at temperature $T = 0$ the leading infrared behavior of their sum reads,

$$\Sigma_f^{(L,a)}(\omega) + \Sigma_f^{(L,b)}(\omega) \stackrel{\omega \rightrightarrows 0}{=} (-1)^{3L-1+L_{sp}} N^{L_{sp}} M^{L_{ch}} \Gamma^L \times \qquad \text{(A.3)}$$

$$\int_{-\omega}^{0} \frac{d\varepsilon_1}{\pi} \ldots \frac{d\varepsilon_L}{\pi}\, F(\omega, \{\varepsilon_j\})\, [G_f(\bar{\omega}+\omega'+\omega_1) G_b(\bar{\omega}+\omega'+\omega_1+\omega_2) - G_f(\bar{\omega}+\omega'+\omega_3) G_b(\bar{\omega}+\omega'+\omega_3+\omega_2)]$$

Here $\bar{\omega}$ denotes the sum of all frequencies ω, ε_j entering the diagrammatic part, Fig. 9, from the left, and $F(\omega, \{\varepsilon_j\})$ consists of all terms which are not altered by interchanging the c–electron lines. In the infrared limit, $\omega_1 - \omega_3 \to 0$, the term in square brackets may be written as

$$\frac{d}{d\bar{\omega}} [G_f(\bar{\omega}+\omega') G_b(\bar{\omega}+\omega'+\omega_2)](\omega_1 - \omega_3) \tag{A.4}$$

and upon performing the integrations over ω_1, ω_3 the difference $(\omega_1 - \omega_3)$ leads to an additional factor of ω. A similar cancellation of the leading infrared singularity occurs between the terms shown in Fig. 9(c), (d). In an analogous way it may be shown that combining the terms Fig. 9 (a)–(d) leads to a factor of ω^2 compared to the power counting result for one single term. Thus, the infrared singularity of all non–CTMA terms of loop order L is weaker than the Lth order CTMA terms by at least $O(\omega^2)$,

$$\Sigma_{f,b}^{(L,a)}(\omega) + \ldots + \Sigma_{f}^{(L,d)}(\omega) \overset{\omega \to 0}{\propto} \omega^{\alpha_{f,b} + L(1-\alpha_f-\alpha_b)+2}. \tag{A.5}$$

It should be emphasized that in the above derivation, L appears only as a parameter and, thus, the cancellation theorem holds for arbitrarily high loop order L. This proves that the CTMA captures the leading and subleading infrared singularities ($\omega \to 0$) at any given order L.

B. CTMA equations

In this appendix we give explicitly the self–consistent equations which determine the auxiliary particle self–energies within CTMA. For that purpose, it is useful to define conduction electron–fermion and conduction electron–boson vertex functions $T^{(cf)\,(\pm)}$, $T^{(cb)\,(\pm)}$ without (+) or with (−) an alternating sign between terms with even and odd number of rungs (compare Fig. 3). In the Matsubara representation, these vertex functions, to be labelled "even" (+) and "odd" (−) below, are given by the following Bethe–Salpeter equations:

$$T^{(cf)\,(\pm)\,\mu}_{\sigma,\tau}(i\omega_n, i\omega_n', i\Omega_n) = U^{(cf)\,\mu}_{\sigma,\tau}(i\omega_n, i\omega_n', i\Omega_n) \pm V^2 \frac{1}{\beta} \sum_{\omega_n''} G_{b\bar{\mu}}(i\omega_n + i\omega_n'' - i\Omega_n) \times \tag{B.1a}$$

$$G_{f\sigma}(i\omega_n'')\; G^0_{c\mu\tau}(i\Omega_n - i\omega_n'')\; T^{(cf)\,(\pm)\,\mu}_{\tau,\sigma}(i\omega_n'', i\omega_n', i\Omega_n)$$

$$U^{(cf)\,\mu}_{\sigma,\tau}(i\omega_n, i\omega'_n, i\Omega_n) = -V^4 \frac{1}{\beta} \sum_{\omega''_n} G_{b\bar{\mu}}(i\omega_n + i\omega''_n - i\Omega_n) \times \qquad \text{(B.1b)}$$
$$G_{f\sigma}(i\omega''_n)\; G^0_{c\mu\tau}(i\Omega_n - i\omega''_n)\; G_{b\bar{\mu}}(i\omega'_n + i\omega''_n - i\Omega_n)$$

and

$$T^{(cb)\,(\pm)\sigma}_{\mu,\nu}(i\omega_n, i\omega'_n, i\Omega_n) = U^{(cb)\,\sigma}_{\mu,\nu}(i\omega_n, i\omega'_n, i\Omega_n)$$
$$\pm V^2 \frac{1}{\beta} \sum_{\omega''_n} G_{f\sigma}(i\omega_n + i\omega''_n - i\Omega_n) \times \qquad \text{(B.2a)}$$
$$G_{b\bar{\mu}}(i\omega''_n)\; G^0_{c\nu\sigma}(i\omega''_n - i\Omega_n)\; T^{(cb)\,(\pm)\sigma}_{\nu,\mu}(i\omega''_n, i\omega'_n, i\Omega_n)$$
$$U^{(cb)\,\sigma}_{\mu,\nu}(i\omega_n, i\omega'_n, i\Omega_n) = -V^4 \frac{1}{\beta} \sum_{\omega''_n} G_{f\sigma}(i\omega_n + i\omega''_n - i\Omega_n) \times \qquad \text{(B.2b)}$$
$$G_{b\bar{\mu}}(i\omega''_n)\; G^0_{c\nu\sigma}(i\omega''_n - i\Omega_n)\; G_{f\sigma}(i\omega'_n + i\omega''_n - i\Omega_n).$$

Note that, in addition to the alternating sign, these vertex functions differ from the T–matrices defined in Eqs. (5.1), (5.2) in that they contain only terms with two or more rungs, since the inhomogeneous parts $U^{(cf)}$ and $U^{(cb)}$ represent terms with two bosonic or fermionic rungs, respectively. The terms with a single rung correspond to the NCA diagrams and are evaluated separately (see below).

The spin degrees of freedom of $T^{(cf)\,(\pm)}$ are uniquely determined by the spin indices σ, τ of the ingoing conduction electron and pseudofermion lines (Fig. 3). It is instructive to note that in the spin $S = 1/2$ case ($N = 2$) the singlet and triplet vertex functions (which correspond to the two–particle Green's functions in the singlet channel, $\phi^{\,s} \sim \sum_\sigma \langle T\{(c_\sigma f_{-\sigma} - c_{-\sigma} f_\sigma)(c^\dagger_\sigma f^\dagger_{-\sigma} - c^\dagger_{-\sigma} f^\dagger_\sigma)\}\rangle$, and in the triplet channel with magnetic quantum number $m = 0, \pm 1$, $\phi^{\,t}_{m=0} \sim \sum_\sigma \langle T\{(c_\sigma f_{-\sigma} + c_{-\sigma} f_\sigma)(c^\dagger_\sigma f^\dagger_{-\sigma} + c^\dagger_{-\sigma} f^\dagger_\sigma)\}\rangle$, $\phi^{\,t}_{m=\pm 1} \sim \langle T\{c_{\pm\frac{1}{2}} f_{\pm\frac{1}{2}} c^\dagger_{\pm\frac{1}{2}} f^\dagger_{\pm\frac{1}{2}}\}\rangle$, respectively) may be identified in the following way,

$$T^{(cf)\,s} = \sum_\sigma T^{(cf)\,(-)}_{\sigma,-\sigma} \qquad \text{(B.3a)}$$
$$T^{(cf)\,t}_{m=0} = \sum_\sigma T^{(cf)\,(+)}_{\sigma,-\sigma} \qquad \text{(B.3b)}$$
$$T^{(cf)\,t}_{m=\pm 1} = \quad T^{(cf)\,(+)}_{\pm\frac{1}{2},\pm\frac{1}{2}}. \qquad \text{(B.3c)}$$

Analogous relations hold for the conduction electron–boson vertex function in terms of the channel degrees of freedom μ, ν. The total CTMA pseudoparticle self–energies, as derived by functional differentiation from the

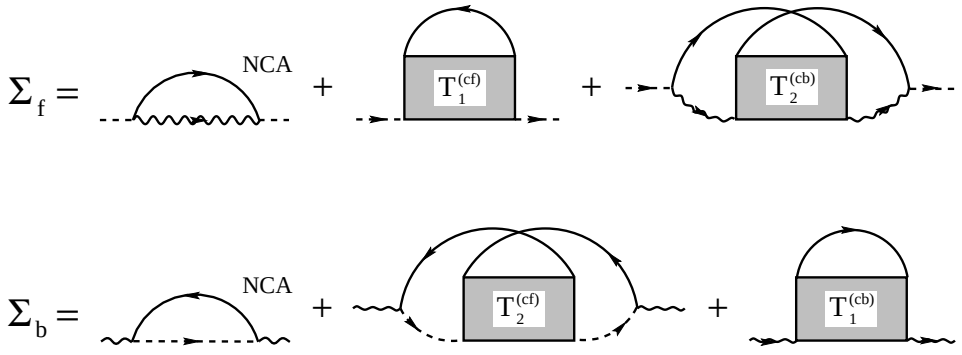

Fig. 10. Diagrammatic representation of the CTMA expressions for pseudoparticle self–energies Σ_f and Σ_b. The first term drawn on the righthand side of Σ_f and Σ_b, respectively, is the NCA diagram. The diagrammatic parts $T_{1,2}^{(cf)}$, $T_{1,2}^{(cb)}$ are explained in the text.

generating functional Φ, Fig. 5, are shown in Fig. 10 and consist of three terms each,

$$\Sigma_{f\sigma}(i\omega_n) \;=\; \Sigma_{f\sigma}^{(NCA)}(i\omega_n) + \Sigma_{f\sigma}^{(cf)}(i\omega_n) + \Sigma_{f\sigma}^{(cb)}(i\omega_n) \tag{B.4}$$

$$\Sigma_{b\bar{\mu}}(i\omega_n) \;=\; \Sigma_{b\bar{\mu}}^{(NCA)}(i\omega_n) + \Sigma_{b\bar{\mu}}^{(cf)}(i\omega_n) + \Sigma_{b\bar{\mu}}^{(cb)}(i\omega_n)\;. \tag{B.5}$$

The first term of Σ_f and Σ_b represents the NCA self–energies, Eqs. (4.2a), (4.2b). The second and third terms arise from the spin and the charge fluctuations, respectively, and are given for pseudofermions by

$$\Sigma_{f\sigma}^{(cf)}(i\omega_n) \;=\; M\,\frac{1}{\beta}\sum_{\Omega_n} G_c^0(i\Omega_n - i\omega_n) T_1^{(cf)}(i\omega_n, i\omega_n, i\Omega_n) \tag{B.6a}$$

$$\begin{aligned}\Sigma_{f\sigma}^{(cb)}(i\omega_n) \;=\; & -M\,V^2 \frac{1}{\beta^2}\sum_{\omega_n'\omega_n''} G_c^0(i\omega_n - i\omega_n') G_b(i\omega_n') \times \\ & T_2^{(cb)}(i\omega_n', i\omega_n'', i\omega_n' + i\omega_n'' - i\omega_n) G_c^0(i\omega_n - i\omega_n'') G_b(i\omega_n'')\end{aligned} \tag{B.6b}$$

and for slave bosons by

$$\begin{aligned}\Sigma_{b\bar{\mu}}^{(cf)}(i\omega_n) \;=\; & -N\,V^2 \frac{1}{\beta^2}\sum_{\omega_n'\omega_n''} G_c^0(i\omega_n' - i\omega_n) G_f(i\omega_n') \times \\ & T_2^{(cf)}(i\omega_n', i\omega_n'', i\omega_n' + i\omega_n'' - i\omega_n) G_c^0(i\omega_n'' - i\omega_n) G_f(i\omega_n'')\end{aligned} \tag{B.7a}$$

$$\Sigma_{b\bar{\mu}}^{(cb)}(i\omega_n) \;=\; N\,\frac{1}{\beta}\sum_{\Omega_n} G_c^0(i\omega_n - i\Omega_n) T_1^{(cb)}(i\omega_n, i\omega_n, i\Omega_n)\;, \tag{B.7b}$$

where the vertex functions appearing in these expressions are defined as

$$T_1^{(cf)} = \frac{N+1}{2}\, T^{(cf)\,(+)} + \frac{N-1}{2}\, T^{(cf)\,(-)} - N\, U^{(cf)} \tag{B.8a}$$

$$T_2^{(cf)} = \frac{N+1}{2}\, T^{(cf)\,(+)} - \frac{N-1}{2}\, T^{(cf)\,(-)} - U^{(cf)} \tag{B.8b}$$

$$T_1^{(cb)} = \frac{M-1}{2}\, T^{(cb)\,(+)} + \frac{M+1}{2}\, T^{(cb)\,(-)} - M\, U^{(cb)} \tag{B.9a}$$

$$T_2^{(cb)} = \frac{M-1}{2}\, T^{(cb)\,(+)} - \frac{M+1}{2}\, T^{(cb)\,(-)} - U^{(cb)}\ . \tag{B.9b}$$

These combinations of the even and odd vertex functions ensure the proper spin and channel summations in the self–energies. For the sake of clarity, the spin and channel indices as well as the frequency variables are not shown explicitly. In Eqs. (B.8a), (B.9a) the terms with two rungs, $N\,U^{(cf)}$, $M\,U^{(cb)}$, have been subtracted, since they would generate non–skeleton self–energy diagrams. Likewise, in Eqs. (B.8b), (B.9b) the two–rung terms have been subtracted in order to avoid a double counting of terms in the self–energies.

We now turn to the analytic continuation to real frequencies of the expressions derived above. Transforming the Matsubara summations into contour integrals shows that integrations along branch cuts of auxiliary particle Green's functions carry an additional factor $\exp(-\beta\lambda)$ as compared to integrations along branch cuts of physical Green's functions, which vanishes upon projection onto the the physical Fock space, $\lambda \to \infty$. Thus, as a general rule, only integrations along branch cuts of the c–electron propagators contribute to the auxiliary particle self–energies. Therefore, by performing the analytic continuation, $i\omega_n \to \omega - i0 \equiv \omega$ in all frequency variables, we obtain the advanced pseudofermion self–energy,

$$\Sigma_{f\sigma}^{(cf)}(\omega) = M \int \frac{d\varepsilon}{\pi}\, f(\varepsilon-\omega)\, A_c^0(\varepsilon-\omega)\, \pi\mathcal{N}(0) T_1^{(cf)}(\omega,\omega,\varepsilon) \tag{B.10a}$$

$$\Sigma_{f\sigma}^{(cb)}(\omega) = -M\,\Gamma \int \frac{d\varepsilon}{\pi} \int \frac{d\varepsilon'}{\pi}\, f(\varepsilon-\omega)\, f(\varepsilon'-\omega)\ \times \tag{B.10b}$$

$$A_c^0(\omega-\varepsilon) G_b(\varepsilon)\, \pi\mathcal{N}(0) T_2^{(cb)}(\varepsilon,\varepsilon',\varepsilon+\varepsilon'-\omega) A_c^0(\omega-\varepsilon') G_b(\varepsilon')$$

and the advanced slave boson self–energy,

$$\Sigma_{b\bar{\mu}}^{(cf)}(\omega) = -N\,\Gamma \int \frac{d\varepsilon}{\pi} \int \frac{d\varepsilon'}{\pi}\, f(\varepsilon-\omega)\, f(\varepsilon'-\omega)\ \times \tag{B.11a}$$

$$A_c^0(\varepsilon-\omega) G_f(\varepsilon)\, \pi\mathcal{N}(0) T_2^{(cf)}(\varepsilon,\varepsilon',\varepsilon+\varepsilon'-\omega) A_c^0(\varepsilon'-\omega) G_f(\varepsilon')$$

$$\Sigma_{b\bar{\mu}}^{(cb)}(\omega) = -N \int \frac{d\varepsilon}{\pi}\, f(\varepsilon-\omega)\, A_c^0(\omega-\varepsilon)\, \pi\mathcal{N}(0) T_1^{(cb)}(\omega,\omega,\varepsilon), \tag{B.11b}$$

where the vertex functions are given by Eqs. (B.8), (B.9) with

$$T^{(cf)\,(\pm)\,\mu}_{\sigma,\tau}(\omega,\omega',\Omega) \;=\; U^{(cf)\,(\pm)\,\mu}_{\sigma,\tau}(\omega,\omega',\Omega)$$
$$\pm(-\Gamma)\int\frac{d\varepsilon}{\pi}\;f(\varepsilon-\Omega)\;\times \tag{B.12a}$$
$$G_{b\bar{\mu}}(\omega+\varepsilon-\Omega)G_{f\sigma}(\varepsilon)A^0_{c\mu\tau}(\Omega-\varepsilon)T^{(cf)\,(\pm)\,\mu}_{\tau,\sigma}(\varepsilon,\omega',\Omega)$$
$$\pi\mathcal{N}(0)\;U^{(cf)\,(\pm)\,\mu}_{\sigma,\tau}(\omega,\omega',\Omega) \;=\; +\Gamma^2\int\frac{d\varepsilon}{\pi}\;f(\varepsilon-\Omega)\;\times \tag{B.12b}$$
$$G_{b\bar{\mu}}(\omega+\varepsilon-\Omega)G_{f\sigma}(\varepsilon)A^0_{c\mu\tau}(\Omega-\varepsilon)G_{b\bar{\mu}}(\omega'+\varepsilon-\Omega)$$

and

$$T^{(cb)\,(\pm)\sigma}_{\mu,\nu}(\omega,\omega',\Omega) \;=\; U^{(cb)\,(\pm)\sigma}_{\mu,\nu}(\omega,\omega',\Omega)$$
$$\pm(+\Gamma)\int\frac{d\varepsilon}{\pi}\;f(\varepsilon-\Omega)\;\times \tag{B.13a}$$
$$G_{f\sigma}(\omega+\varepsilon-\Omega)G_{b\bar{\mu}}(\varepsilon)A^0_{c\nu\sigma}(\varepsilon-\Omega)\;T^{(cb)\,(\pm)\sigma}_{\nu,\mu}(\varepsilon,\omega',\Omega)$$
$$\pi\mathcal{N}(0)\;U^{(cb)\,(\pm)\sigma}_{\mu,\nu}(\omega,\omega',\Omega) \;=\; -\Gamma^2\int\frac{d\varepsilon}{\pi}\;f(\varepsilon-\Omega)\;\times \tag{B.13b}$$
$$G_{f\sigma}(\omega+\varepsilon-\Omega)G_{b\bar{\mu}}(\varepsilon)A^0_{c\nu\sigma}(\varepsilon-\Omega)\;G_{f\sigma}(\omega'+\varepsilon-\Omega)$$

In the above expressions, like in the NCA equations (4.2), we have used the dimensionless conduction electron spectral density, $A^0_c(\omega)=\frac{1}{\pi}\,\mathrm{Im}G^0_{c\mu\sigma}(\omega-i0)/\mathcal{N}(0)$, and we have suppressed obvious spin and channel indeces. All frequency variables are to be understood as the limit $\omega\equiv\omega-i0$.
The equations (B.10), (B.11), supplemented by the vertex functions Eqs. (B.8), (B.9), (B.12), (B.13) form, together with the NCA contributions Eqs. (4.2a), (4.2b) and the definitions of the auxiliary particle Green's functions, Eqs. (3.10), (3.11), the closed set of self–consistent CTMA equations [52]. It is seen that in these equations only those branches of the T–matrix vertex functions appear which are advanced with respect to all three frequency variables, although in general the T–matrix consists of 2^3 independent analytical branches. This simplification is a consequence of the exact projection onto the physical sector of Fock space. Inspection of the analytically continued CTMA equations also shows that the slave boson self–energy is obtained from the pseudofermion self–energy, including the proper signs, by simply replacing $G_f\leftrightarrow G_b$ and inverting the frequency argument of A^0_c in all expressions.

Eqs. (B.10)–(B.13) may be rewritten in terms of the spectral functions without threshold, $\tilde{A}_{f,b}$, in a straight–forward way as explained in section 4.3, thus avoiding divergent statistical factors in the d–electron Green's

function. The CTMA equations are solved numerically by iteration. In each iteration step the NCA and the T–matrix contributions are computed separetely. We solve the linear T–matrix Bethe–Salpeter–Equations (B.12), (B.12) by discretization of the frequency integrals and subsequent solution of the resulting multidimensional linear equations. Because of the formulation given above, where first the vertex parts $T^{(cf)\,(\pm)}$ and $T^{(cf)\,(\pm)}$, comprised of all T–matrix diagrams with two or more rungs, are calculated and in a second step the non–skeleton two–rung contributions are subtracted (Eqs. (B.8), (B.9)), each term of the T–matrix equations involves at most one frequency integration. The resulting numerical effort is manageable: One complete iteration within the self–consistent scheme has been done on a parallel computer within approximately 5–10 s CPU time.

REFERENCES

[1] L.D. Landau, Sov.Phys. JETP **3**, 920 (1956); **5**, 101 (1957); **8**, 70 (1959).

[2] A. J. Millis, Phys. Rev. B **48**, 7183 (1993).

[3] T. Moriya and T. Takimoto, J. Phys. Soc. Japan **64**, 960 (1995)

[4] A. Rosch et al., Phys. Rev. Lett. **79**, 159 (1997).

[5] For non–FL behavior near a quantum spin–glass transition, see S. Sachdev, N. Read and R. Oppermann, Phys. Rev. B **52**, 10286 (1995).

[6] H. v. Löhneysen et al., Phys. Rev. Lett. **72**, 3262 (1994); B. Bogenberger and H. v. Löhneysen, Phys. Rev. Lett. **74**, 1016 (1995).

[7] H. v. Löhneysen, J. Phys. Cond. Mat. **8** 9689 (1996).

[8] F. Steglich, J. Phys. Cond. Mat. **8** 9909 (1996).

[9] F. M. Grosche, S. R. Julian, N. D. Mathur and G. G. Lonzarich, Physica B **223**+**224**, 50 (1996).

[10] S. R. Julian et al., J. Phys. Cond. Mat. **8** 9675 (1996).

[11] P. Nozierès and A. Blandin, J. Phys. (Paris) **41**, 193 (1980).

[12] A comprehensive overview appears in D. L. Cox and F. Zawadowski, Adv. Phys., in press (1998); (cond-mat/9704103).

[13] D.L. Cox, Phys. Rev. Lett. **59**, 1240 (1987); Physica C 153, 1642 (1988).

[14] M. B. Maple et al., J. Low Temp. Phys. **95**, 225 (1994); **99**, 223 (1995); M. B. Maple et al., J. Phys. Cond. Mat. **8** 9773 (1996).

[15] R. Chain and M. B. Maple, J. Phys. Cond. Mat. **8** 9939 (1996).

[16] J. R. Schrieffer and P. A. Wolff, Phys. Rev. B **149**, 491 (1966).

[17] K. G. Wilson, Rev. Mod. Phys. **47**, 773 (1975).

[18] N. Andrei, K. Furuya, J.H. Löwenstein, Rev.Mod.Phys. **55**, 331 (1983).

[19] P.B. Wiegmann, A.M. Tsvelik, Pis'ma Zh. Eksp. Teor. Fiz. **38**, 489 (1983) [JETP Lett. **38**, 591 (1983)].

[20] P. Nozières, J. Low. Temp. Phys. **17**, 31 (1974).

[21] N. Andrei, C. Destri, Phys. Rev. Lett. **52**, 364, (1984).

[22] A. M. Tsvelik, J. Phys. C **18** 159 (1985).

[23] I. Affleck and A.W.W. Ludwig, Nucl. Phys. **352**, 849, (1991); **B360**, 641, (1991); Phys. Rev. B **48**, 7297 (1993).

[24] S. E. Barnes, J. Phys. **F6**, 1375 (1976); **F7**, 2637 (1977).

[25] A. A. Abrikosov, Physics **2**, 21 (1965).

[26] P. Coleman, *Phys. Rev.* **B29**, 3035 (1984).

[27] K. Yamada, Prog. Theor. Phys. **53**, 970 (1975); *ibid.* **54**, 316 (1975); *ibid.* **55**, 1345 (1976); K. Yosida and K. Yamada, Prog. Theor. Phys. **53**, 1286 (1975).

[28] D. L. Cox, N. E. Bickers and J. W. Wilkins, Phys. Rev. B **36**, 2036 (1987).

[29] P. W. Anderson, Phys. Rev. Lett. **18**, 1049 (1967).

[30] P. Nozières and C. T. De Dominicis, Phys. Rev. **178**, 1073; 1084; 1097 (1969).

[31] G. D. Mahan, *Many–Particle Physics*, 2nd ed., pp. 732 (Plenum Press, New York, 1990) gives an overview.

[32] K. D. Schotte and U. Schotte, Phys. Rev. **185**, 509 (1969).

[33] B. Menge and E. Müller–Hartmann, Z. Phys. **B73**, 225 (1988).

[34] T.A. Costi, P. Schmitteckert, J. Kroha and P. Wölfle, Phys. Rev. Lett. **73**, 1275 (1994).

[35] T.A. Costi, P. Schmitteckert, J. Kroha and P. Wölfle, Physica (Amsterdam) **235–240C**, 2287 (1994).

[36] S. Fujimoto, N. Kawakami and S.K. Yang, J.Phys.Korea **29**, S136 (1996).

[37] D. M. Newns and N. Read, J. Phys. **C16**, 3273 (1983); Adv. Phys. **36**, 799 (1988).

[38] S. Elitzur, Phys. Rev. D **12**,3978 (1975).

[39] A. Jevicki, Phys. Lett. B **71**, 327 (1977).

[40] F. David, Comm. Math. Phys. **81**, 149 (1981).

[41] I.D. Lawrie, J. Phys. A **18**, 1141 (1985).

[42] B. Jin and Y. Kuroda, J. Phys. Soc. Japan **57**, 1687 (1988).

[43] T. Matsuura et al., J. Phys. Soc. Japan **66**, 1245 (1997).

[44] G. Baym and L.P. Kadanoff, Phys. Rev. **124**, 287 (1961); G. Baym, Phys. Rev. **127** 1391 (1962).

[45] H. Keiter and J. C. Kimball, J. Appl. Phys. **42**, 1460 (1971); N. Grewe and H. Keiter, Phys. Rev B **24**, 4420 (1981).

[46] Y. Kuramoto, Z. Phys. B **53**, 37 (1983); H. Kojima, Y. Kuramoto and M Tachiki, *ibid.* **54**, 293 (1984); Y. Kuramoto and H. Kojima, *ibid.* **57**, 95, (1984); Y. Kuramoto, *ibid.* **65**, 29, (1986).

[47] E. Müller–Hartmann, *Z. Phys.* **B57**, 281 (1984).

[48] T.A. Costi, J. Kroha, and P. Wölfle, PRB **53**, 1850 (1996).

[49] N. E. Bickers, *Rev. Mod. Phys.* **59**, 845 (1987); N. E. Bickers, D. L. Cox & J. W. Wilkins, *Phys. Rev.* **B36**, 2036 (1987).

[50] D. L. Cox and A. E. Ruckenstein, Phys. Rev. Lett. **71**, 1613 (1993).

[51] F. Anders and N. Grewe, Europhys. Lett. **26**, 551 (1994); F. Anders, J. Phys. Cond. Mat. **7**, 2801 (1995).

[52] J. Kroha, P. Wölfle and T. A. Costi, Phys. Rev. Lett. **79**, 261 (1997).